Journal of Energy Storage 70 (2023) 107890

Contents lists available at ScienceDirect

Journal of Energy Storage

journal homepage: www.elsevier.com/locate/est

Research papers

Influence of strong bromine binding complexing agent in electrolytes on the performance of hydrogen/bromine redox flow batteries

Michael Küttinger [a,b,*], Kobby Saadi [c], Théo Faverge [a], Nagaprasad Reddy Samala [c], Ilya Grinberg [c], David Zitoun [c], Peter Fischer [a]

[a] Department of Applied Electrochemistry, Fraunhofer Institute for Chemical Technology ICT, Joseph-von-Fraunhofer-Strasse 7, D-76327 Pfinztal, Germany
[b] Institute for Mechanical Process Engineering and Mechanics, Karlsruhe Institute of Technology KIT, Strasse am Forum 8, D-76131 Karlsruhe, Germany
[c] Department of Chemistry, Faculty of Exact Sciences, Bar-Ilan University, 5290002 Ramat Gan, Israel

ARTICLE INFO

Keywords:
Redox flow battery
Ionic liquid
Bromine
Bromine complexing agent
Battery performance

ABSTRACT

1-*n*-Hexylpyridin-1-ium bromide [C6Py]Br is investigated in this work as bromine complexing agent (BCA) in aqueous bromine electrolytes on its influence on hydrogen bromine redox flow battery (H_2/Br_2-RFB) performance. $[C6Py]^+$-cations bind bromine of aqueous polybromide solutions safely in an additional fused salt phase limiting the vapor pressure of Br_2. Dissolved in aqueous electrolyte solutions, however, $[BCA]^+$ cations drastically lower PFSA membranes' conductivity in the H_2/Br_2-RFB. In this work the combination of the very strong bromine-binding $[C6Py]^+$cation and an excess of bromine in the electrolyte lead to an almost complete absorption of 99.6 mol% $[C6Py]^+$ into the fused salt within the electrolyte's operation range. In comparison to similar application of short side chain 1-ethylpyridinium bromide, adverse effects are stronger compensated by use of [C6Py]Br. Increases in membrane resistance of the membrane in contact with $[C6Py]^+$ cations are reversible in contrast for contact with $[C2Py]^+$ cations. Electrolytes are cycled for at least 12 cycles and offer a stable useable capacity of 176.7 Ah L^{-1} and reach and stable discharge energy densities of 138.91 Wh L^{-1}. Strong bromine binding properties between $[C6Py]^+$ cations and polybromides are confirmed by DFT studies. In contrast to $[C2Py]^+$ electrolytes, the long-chain $[C6Py]^+$ cation in electrolytes has a higher cycling stability or a low decrease in capacity and energy density.

1. Introduction

Hydrogen-bromine redox flow batteries (H_2/Br_2-RFB) are most promising candidates among redox flow batteries for industrial scale energy storage alongside all-vanadium redox flow batteries and zinc/bromine redox flow batteries (Zn/Br_2-RFB) [1–5]. Advantages of the H_2/Br_2-RFB are the fast kinetics of the bromine/bromide redox couple in the positive half cell [1,6–9] and of the hydrogen/proton redox couple in the negative half cell [1,8,9]. For charge and discharge operation a single converter unit is applied, consisting of a gas diffusion electrode in the negative hydrogen half cell [10] and a flow through, flow by or mixed electrode operated with liquid electrolytes for the positive bromine half cell [1,6,11–13] (Fig. 1a). Two storage systems for liquid aqueous bromine electrolytes and gaseous hydrogen [8,10,14] are connected to the converter (Fig. 1a). Bromine electrolytes consist of hydrobromic acid (HBr) and bromine (Br_2) in aqueous solution and are pumped through the positive half cell electrode [11,12,15]. During charge, bromide is oxidized to bromine and vice versa during discharge [10,16,17].

In order to limit volatility of the harmful Br_2 [18], organic ammonium cations are used to reduce the vapor pressure [19,20]. Unfortunately, these cations reduce the conductivity of applied PFSA membranes [12,21,22] and lead to the accumulation of a second and poorly conductive phase in the converter cells [12]. Electrolytes containing high amounts of Br_2 are quite safe for use and help to reduce the effects of both drawbacks [15]. To further reduce the impact of these disadvantages and to increase the performance of the H_2/Br_2-RFB, the strongly Br_2-binding cation 1-*n*-hexylpyridin-1-ium $[C6Py]^+$ [19,23] is used as additive for the first time in a cycling test. The combination of the very strong Br_2-binding additive $[C6Py]^+$ with improved electrolyte formulation shall lead to larger cycle stability in terms of stable and higher useable electrolyte capacities, higher useable energy densities and stable membrane conductivity compared to electrolytes using the

* Corresponding author at: Department of Applied Electrochemistry, Fraunhofer Institute for Chemical Technology ICT, Joseph-von-Fraunhofer-Strasse 7, D-76327 Pfinztal, Germany.
E-mail address: michael.kuettinger@gmx.de (M. Küttinger).

https://doi.org/10.1016/j.est.2023.107890
Received 27 July 2022; Received in revised form 23 February 2023; Accepted 31 May 2023
Available online 22 June 2023

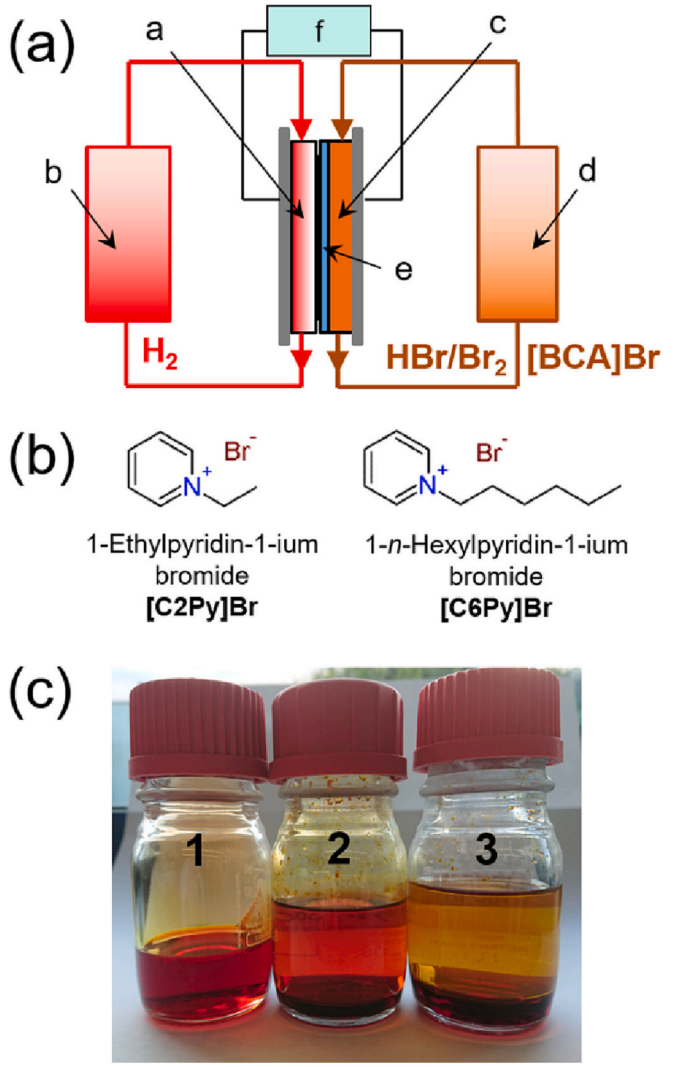

Fig. 1. (a) Scheme of a H_2/Br_2-RFB with a single battery cell in the centre, built up from "a" the hydrogen gas diffusion electrode and "c" the aqueous bromine flow half cell, which are connected via "e" a Nafion117 membrane. The aqueous bromine electrolyte is pumped through the cell and stored in a tank "d", while hydrogen is ideally stored in "b". "f" represents the load/grid that charges the battery or to which the battery releases energy. In (b), the structures of the BCAs 1-ethylpyridin-1-ium bromide [C2Py]Br and of 1-*n*-hexylpyridin-1-ium bromide [C6Py]Br are shown. In (c), electrolytes are shown in a photography, all having the same concentrations (1.11 M Br_2, 5.47 M HBr). Glass "1" shows a BCA-free electrolyte, while in glass "2" the electrolyte contains 1.11 M [C2Py]Br and glass contains "3" 1.11 M [C6Py]Br. It can be seen that in glass "1" there is some bromine vapor above the solution in the gas phase, which is not the case in "2" and "3". In "2" and "3" there is a fused salt in both cases at the bottom of the glasses. From the colouration of the aqueous solutions, it can be observed that [C6Py]Br binds (yellow colour) the bromine more strongly in the fused salt than [C2Py]Br (brown colour). (For interpretation of the references to colour in this figure legend, the reader is referred to the web version of this article.)

moderate Br_2-binding 1-ethylpyridin-1-ium $[C2Py]^+$ in earlier works [12,15] from our group.

1.1. State of the art

Br_2 forms soluble polybromides (Br^-_{2n+1}) in contact with bromide in acidic aqueous solutions of HBr used as electrolytes in H_2/Br_2-RFB [11,16,24–33]. Increased solubility up to 7.96 M Br_2 in 2.85 M HBr solution [11] allows aqueous HBr/Br_2 solutions to be cycled in H_2/Br_2-RFB with electrolytes reaching a capacity of 179.6 Ah L^{-1} [11]. Employing low-cost aqueous HBr 48 wt% solutions available in industrial quantity and technical purity, the concentration limits of HBr/Br_2 electrolytes have been defined for the state of charge (*SoC*) in the past [11]: *SoC* 0 % corresponds to c(HBr) = 7.7 M and *SoC* 100 % corresponds to c(HBr) = 1 M and $c(Br_2)$ = 3.35 M [11]. These concentration limitations base on cycling performance in a H_2/Br_2-RFB single cell in combination with avoiding electrolyte separation due to limited solubility of Br_2 and to reach large electrolyte conductivities (κ) of $\kappa \geq 298$ mS cm^{-1} [11].

The harmful Br_2 has a high vapor pressure (202–211 mmHg at ϑ = 25 °C [18,34,35]) and is also volatile from aqueous solutions depending on the mixing ratio of bromine and bromide [1,10]. In electrolytes of Zn/Br_2-RFB, vanadium/bromine-RFB and H_2/Br_2-RFB, quaternary ammonium bromides are applied as bromine complexing agents (BCA) [2,12,19,21,23,29,36–50] to reduce bromines' vapor pressure [20]. BCAs increase heat of vaporization of Br_2 by 1.3 to 2.3 times (calculated from [18,20]) and cause a strong reduction of Br_2 concentration of by least 70 mol% Br_2 in the aqueous electrolyte phase compared to BCA-free electrolytes [19]. The organic $[BCA]^+$ cation is only slightly soluble in aqueous solution (aq) containing polybromides and precipitates as $[BCA]Br_{2n+1}$ salt [19,36]. Br_2 is bound strongly in this fused salt (fs) [23]. The solubility equilibrium is shown for the example of 1-*n*-hexylpyridin-1-ium bromide [C6Py]Br in Eq. (1) [29,36,37,45,51]:

$$[C6Py]^+(aq) + Br_{2n+1}{}^-(aq) \rightleftharpoons [C6Py]Br_{2n+1}(fs)\downarrow \quad (1)$$

Some of the BCAs investigated, such as 1-ethylpyridin-1-ium bromide [C2Py]Br (Fig. 1b) and 1-*n*-hexylpyridin-1-ium bromide [C6Py]Br (Fig. 1b) form a liquid fused salt (fs) [19,23,37,38], which is stored underneath the aqueous phase [19,36,41,43] (Fig. 1c) due to a large difference in densities between the two phases [19,23].

For safe application $[BCA]^+$ cations offer high binding strength towards Br_2 in the fused salt [19,23] and in parallel a sufficient Br_2 concentration in aqueous phase for a powerful discharge operation of the cell [12,19]. At first sight, both conditions are contradictory and require a compromise. The high safety of electrolytes has already been demonstrated in detail by a strong decrease of Br_2 concentrations in aqueous electrolyte solution applying BCAs [19,43]. In solutions of 5.45 M HBr/1.11 M Br_2 and 1.11 M [BCA]Br (≈*SoC* 33 %), [C2Py]Br as BCA binds 88.8 mol% Br_2 in the fused salt and 98.6 mol% Br_2 are bound when employing [C6Py]Br [23]. For higher *SoCs* (e.g. 2.34 M HBr/2.68 M Br_2/ ≈*SoC* 80 %) 90.2 mol% Br_2 for $[C2Py]^+$ and 91.5 mol% Br_2 for $[C6Py]^+$ have been investigated to be stored in the fused salt [23]. The $[C6Py]^+$ cation is a much stronger BCA compared to the $[C2Py]^+$ cation with respect to the *SoC*, which is also visible in electrolytes shown in Fig. 1c. Both BCAs are predestined to be lead to safe electrolytes for application in H_2/Br_2-RFB.

The bromine binding strength of the BCA towards tribromide Br_3^- increases with increasing length of the alkyl side chain from ethyl to *n*-hexyl, while this effect has a minor relevance for binding pentabromide Br_5^- and heptabromide Br_7^- [19,41].

High electrolyte conductivity of BCA-free and BCA-containing aqueous electrolytes between $298.0 \leq \kappa \leq 763.2$ mS cm^{-1} bases predominantly on the high proton concentration [11,19]. In solutions containing $[C2Py]^+$ and $[C6Py]^+$, the electrolyte conductivity decreases due to the organic character and the increasing size of these cations: κ = 461.1 mS cm^{-1} (1.11 M [C2Py]Br in 7.7 M HBr) and κ = 381.1 mS cm^{-1} (1.11 M [C6PyBr] in 7.7 M HBr) in contrast to κ = 703.0 mS cm^{-1} for BCA-free 7.7 M HBr solutions.

The fused salt stores large amounts of Br_2 and is therefore the main bromine energy storage in the electrolyte [23]. However, the fused salt is an anhydrous ionic liquid composed of the $[BCA]^+$ cation and polybromides Br_3^-, Br_5^- and Br_7^- leading to low conductivity κ < 90 mS cm^{-1} and to high viscosities (η) $\eta \geq 13$ mPas compared to the respective aqueous electrolyte [23]. The fused salts are therefore not applied in the

investigated H_2/Br_2-RFB [23].

In the past the influence of BCAs on the performance of a H_2/Br_2-RFB single cell using [C2Py]Br [12,15] was investigated. In cell tests, electrolytes cannot be charged starting from $SoC = 0$ % (7.7 M HBr and 1.11 M $[C2Py]^+$) due to a high ohmic resistance in the cell [12]. However, starting from $SoC = 100$ %, discharge operation is enabled, but severely limited by strong overvoltages occurring during charge and discharge [12]. This initially resulted in a maximum usable capacity of only 53.9 Ah L^{-1} and an energy density of 41.5 Wh L^{-1} [12]. The presence of $[C2Py]^+$ cations in the aqueous electrolyte limits the performance of the positive half cell [12] and the transport of protons in Nafion membranes [12,21]: (1) During charge operation, $[C2Py]^+$ cations and polybromides form liquid fused salt in the bromine half cell [12], which has low conductivity of $\kappa < 90$ mS cm^{-1} [23] and results in sharply rising overvoltages in the positive half cell [12,50]. The formation of fused salt in the positive half cell is fully reversible [12]. In parallel (2), $[C2Py]^+$ cations are released from the fused salt into the aqueous solution during discharge operation. The organic cations diffuse into the PFSA membrane and form addition bonds with sulphonate groups of the membrane [12,21,52]. These hydrophobic $[BCA]^+$ cations displace water molecules from the membrane [53,54]. The membrane dries out and transport of protons is inhibited [21,54] leading to a reduced conductivity of PFSA membranes [12,21,53]. So far rising ohmic resistances have been investigated as a non-reversible process [12]. In addition, (3) crossover of electrolyte intensifies both challenges (1) and (2) leading to low energy density and capacity [12].

Saadi et al. [21] showed that $[C2Py]^+$ cations do no only penetrate and interact with PFSA membranes but also cross over the membrane. PVDF-SiO_2 separators, on the other hand, do not show this interaction with the $[BCA]^+$ cation, but have generally lower performance than PFSA membranes in terms of 50 to 62 % higher membrane resistances in BCA free HBr/Br_2 electrolytes [21]. Saadi et al. [21] further propose to develop specific membranes or separators that provide high membrane performance with low interactions between the membrane and the BCA molecules.

A different and more cost-effective alternative to the development of new separators is a modification of the electrolyte formulation with the objective of permanently binding $[BCA]^+$ cations in the fused salt. By providing an excess of Br_2 in the electrolyte to shift the solubility equilibrium (Eq. (1)) towards the fused salt, Küttinger et al. [15] transferred a large fraction of $[C2Py]^+$ cations into the fused salt phase. An excess of Br_2 with the molar ratio of $n(Br_2)/n([BCA]^+) \geq 2.4$ within the entire *SoC* range leads to a much lower fraction of $[C2Py]^+$(aq) cations in the aqueous phase (<5 mol%) [15]. Low concentrations or absence of $[C2Py]^+$(aq) cations prevent from the formation of low conductive fused salt in the cell and from rising membrane resistances [15]. This advantage made it possible for the first time to achieve a usable capacity of 179.6 Ah L^{-1} and an energy density of maximum 133 Wh L^{-1} (at 100 mA cm^{-2}) using an electrolyte containing BCA [15]. The bromine transfer during the cell test takes place by a pure exchange of bromine between the polybromides according to Eq. (2) at the phase interface in the electrolyte tank according to [15] avoiding the release of $[BCA]^+$ cations. This transfer is an alternative one and has been discussed in detail recently [15] and is shown for the example of [C6Py]Br in Eq. (2):

$$[C6Py]Br_{2n+1}(fs) + Br_{2m-1}{}^{-(aq)} \rightleftharpoons [C6Py]Br_{2n-1}(fs) + Br_{2m+1}{}^{-(aq)} \quad (2)$$

Although high capacity and useful energy density are achieved, capacity decreases by 19.6 % and energy density by 30.0 % within 9 cycles [15]. This trend is caused by a very small amount of $[C2Py]^+$, which is sufficient to block the membrane, and the release of $[C2Py]^+$ from the fused salt into the aqueous phase is favoured by crossover to the drawback of the performance [15]. A specification of a maximum of 5 mol% $[BCA]^+$ being in aqueous solution is not sufficient to achieve long-term cycling stability. The application of a stronger Br_2-binding $[BCA]^+$ cation (e.g. $[C6Py]^+$), which preferably remains completely in the fused phase, is targeted.

While [C2Py]Br as moderate BCA has already been extensively studied [12,15,19,23], studies on the strong Br_2-binding [C6Py]Br as BCA do not go beyond ex situ investigation of the electrolyte properties of aqueous phase [19] and fused salt [23]. These studies [19,23] showed $[C2Py]^+$ cations can be an advantage over $[C6Py]^+$ cations mainly due to their moderate bromine binding strength. However, the combination of [C6Py]Br and an excess amount of bromine in the electrolyte solution has not yet been investigated neither ex situ nor in situ but promises a possibility in reaching stable cycling performance. The goal to permanently store $[C6Py]^+$ cations throughout the *SoC* region in the fused salt phase by using its strong Br_2-binding ability shall lead to stable membrane functionality during cycling. An improvement of performance towards electrolytes with [C2Py]Br is expected. Thereby, a usable capacity of 179.6 Ah L^{-1} shall be achieved again and stable energy densities shall be reached during cycling. At the same time, it has to be investigated whether $[C6Py]^+$ cations penetrate less strongly to the membrane due to their large size and thus whether the membrane resistance is less strongly influenced by $[C6Py]^+$ cations.

1.2. Work plan

A $[BCA]^+$ cation, which binds polybromides more strongly than $[C2Py]^+$ or is hardly soluble in aqueous electrolytes, is targeted in electrolyte development. At the same time, an excess amount of bromine within the entire *SoC* range strongly favours the shift of the equilibrium according to Eq. (1) to form fused salt. The combination of applying an excess amount of bromine and a strong $[BCA]^+$ cation should lead to a moderate Br_2 concentration for good discharge performance.

In this study the application of [C6Py]Br as strong Br_2-binding BCA in bromine posolytes of the H_2/Br_2-RFB with a theoretical capacity of 179.6 Ah L^{-1} is investigated with the aim to transfer and keep $[C6Py]^+$ cations within the whole *SoC* range in the fused salt. For further development and achievement of the objectives, bromine in excess amounts is provided in concentrations of +0.84 M (series no. 2), +1.68 M (series no. 3) and +2.51 M Br_2 (series no. 4) at *SoC* 0 % to the electrolytes. In series no. 1 electrolyte without excess amounts of Br_2 (+0.00 M Br_2) is used. The equilibrium of $[C6Py]^+$ and Br_2 between the aqueous phase and the fused salt is determined for these 4 electrolyte mixtures based on concentration studies for Br_2 and the $[C6Py]^+$. The electrolyte conductivity and the influence of $[C6Py]^+$ cations on the membrane are determined and discussed based on the electrolyte compositions. Cycling performance is investigated by measuring cell voltages and half cell potentials in galvanostatic cycling experiments over 12 cycles and limiting macro-kinetic effects such as mass transport limitation, ohmic cell resistances and kinetics are determined qualitatively. To examine benefits or drawbacks of using the longer alkyl side chain BCA [C6Py]Br, results (concentration, energy density and capacity) are compared with results of electrolytes applying [C2Py]Br as a BCA under same conditions from our previous work [15]. In this context, the previous work does not present results for electrolytes with a bromine excess of +0.84 M Br_2 at *SoC* 0 %, so no direct comparison is possible in this case, but a qualitative comparison is shown in the paper. Density functional theory (DFT) studies are performed to confirm the results of the ex-situ studies of the electrolytes and the cell tests. The change in the Gibbs free energy of the ion pairing between the two $[BCA]^+$ cations ($[C2Py]^+$ and $[C6Py]^+$) interacting with bromide Br^- and polybromides Br_{2n+1}^- (n = 1–3) is investigated. No DFT studies on [C6Py]Br concerning the storage of Br_2 have been reported in the literature and [C2Py]Br has only been studied so far in acetonitrile as a solvent [51].

2. Materials and methods

A detailed version of the section "Materials and methods" is available in the Electronic Supplementary Information (ESI) including methods

and substances. All measurements have been carried out at $\vartheta = 23 \pm 1$ °C.

2.1. Chemicals and composition of the electrolytes

Electrolyte solutions consist of HBr, distilled water and Br_2. The used BCA 1-*n*-hexylpyridin-1-ium bromide [C6Py]Br is synthesized according to ref. [43, 55, 56]. The synthesis of [C6Py]Br is confirmed by ^{1}H NMR and ^{13}C NMR analysis by comparison with NMR shifts from the literature [56,57] and shown in the ESI of this research article.

In all electrolytes and independent of the *SoC* a concentration of 1.11 M [C6Py]Br is present. The absolute concentration of HBr related to the *SoC* of the electrolyte is defined as follows: *SoC* 0 % with 7.7 M HBr and *SoC* 100 % with 1 M HBr. The concentrations of Br_2 in the electrolytes depend on the chosen excess amount of Br_2 at *SoC* 0 % and the *SoC* in series no. 1 to 4, which are defined for *SoC* 0 and 100 % in Table 1.

Electrolyte samples are mixed for all series with a volume (V) of $V =$ 30 mL for *SoC* 0, 10, 20, 30, 33, 40, 50, 60, 66, 70, 80, 90 and 100 % for ex situ investigation of electrolyte composition and conductivity. For ex situ measurements the different electrolyte phases are in equilibrium. Detailed concentrations for all components in these samples are shown in Table S-2 in the ESI. The electrolyte ($V = 90$ mL) investigated in cell test cycling is prepared at *SoC* 100 % with different Br_2 concentration (Table 1).

2.2. $[C6Py]^+$ cation concentration in aqueous electrolytes

Concentrations of $[C6Py]^+$(aq) are investigated by Raman spectroscopy from aqueous electrolyte samples for all electrolyte series and at all 13 *SoCs*. Details on the Raman spectrometer equipment are shown in the ESI. Raman spectra are depicted in Figs. S-7 to S-10 in the ESI. $[C6Py]^+$ leads to a strong single Raman peak signal at a Raman shift ($\widetilde{\nu}$) $\widetilde{\nu} = 1029$ cm^{-1} [58–60]. Comparison of its peak area with the peak area of a reference electrolyte with known $[C6Py]^+$ concentration leads to actual $[C6Py]^+$(aq) concentrations (ESI and refs. [12, 19]).

2.3. Bromine concentration in aqueous phase and fused salt

Bromine concentrations in the aqueous electrolytes are determined for all series and *SoCs* by linear chronoamperometry at a rotating disk electrode under rotation on a glassy carbon working electrode. The potential is reduced from open circuit potential to −1.0 *V* vs. Ag/AgCl/KCl(sat.) reference electrode with a scan rate of −40 mV s^{-1}. For low potentials, Br_2 reduction shows a constant limited current I_{lim}, which is proportional to the Br_2 concentration by Levich equation [61–65]. Concentrations of Br_2 are calculated from limiting currents following Eq. (3) ([$c(Br_2)$] = mol L^{-1}, [I_{lim}] = mA). Calibration of the method is described in detail in the ESI and in refs. [15, 19].

$$c(\mathrm{Br_2(aq)}) = 3.424 \bullet 10^{-3}\ \mathrm{mol\ L^{-1}\ mA^{-1}}\ I_{lim} \quad (3)$$

Table 1
Bromine concentrations defined for four different electrolyte mixtures (series no. 1 to 4) at *SoC* 0 % and *SoC* 100 %.

Electrolyte mixture	Concentration Br_2[a]/M	
	At *SoC* 0 %	At *SoC* 100 %
Electrolyte series no. 1 (+0 % of 3.35 M Br_2 at *SoC* 100 %)	0.00	3.35
Electrolyte series no. 2 (+25 % of 3.35 M Br_2 at *SoC* 100 %)	0.84	4.19
Electrolyte series no. 3 (+50 % of 3.35 M Br_2 at *SoC* 100 %)	1.68	5.03
Electrolyte series no. 4 (+75 % of 3.35 M Br_2 at *SoC* 100 %)	2.51	5.86

[a] Bromine is added to the solutions gravimetrically.

Concentrations of Br_2 in fused salts $c(Br_2(fs))$ are calculated from $c(Br_2(aq))$ and volumes of aqueous phase V(aq) and of corresponding fused salt V(fs) as described in the ESI.

2.4. Conductivities of aqueous electrolytes

Electrolyte conductivities of aqueous electrolyte solutions (all series and all *SoCs*) are determined in a calibrated conductivity cell at $\vartheta = 23 \pm 1$ °C. Details of the conductivity calculations and the determination of the cell constant are explained in the ESI and in refs. [11, 12].

2.5. Comparison of [C6Py]Br electrolyte performance to [C2Py]Br electrolyte performance

Conductivities and compositions of electrolytes containing [C6Py]Br as well as their useable electrolyte capacities and discharge energy densities from cell tests are compared with those of electrolytes containing [C2Py]Br. These values ([C2Py]Br) are not determined in this work, but are taken from our own results in refs. [12, 15] to determine the improvement of the electrolyte with [C6Py]Br compared to [C2Py]Br. All values for electrolytes' energy densities and capacities are related to the total amount of the electrolyte volumes, considering the volumes of the aqueous phase and of the fused salt. Capacities of fused salt in chapter 3.3 are differing and related to fused salt volumes only.

2.6. Crossover of $[C2Py]^+$ and $[C6Py]^+$ cations across Nafion117 membrane

The crossover of $[C2Py]^+$ and $[C6Py]^+$ cations through a Nafion117 membrane is studied in a glass diffusion cell, with a geometric crossover membrane area of 3.2 cm^2. Electrolyte (40 mL) containing 4.5 M HBr and 0.31 M [C2Py]Br or 4.5 M HBr and 0.31 M [C6Py]Br is placed on one side (1) of the membrane and 4.5 M HBr solution (40 mL) is placed on the other side (2) of the membrane in the cell. At different times electrolyte samples are extracted from side (2), diluted 10-fold with 4.5 M HBr and examined with UV–Vis spectroscopy. Peak heights of absorbance at a characteristic wavelength of 260 nm for the $[BCA]^+$ cations are used to calculate $[BCA]^+$ concentrations of side (2). The calibration, UV–Vis calibrations and analyses are shown in Figs. S-3 to S-6 in the ESI. The concentrations of the BCAs on side (2) are calculated and the BCA crossover rate is calculated from those as explained in the ESI.

2.7. FTIR investigation of Nafion117 membranes

Nafion117 membranes, which are soaked in aqueous solutions of [C6Py]Br electrolytes ex situ at all *SoCs* for all 4 electrolyte series, are investigated by Fourier Transform Infrared Spectroscopy (FTIR spectroscopy). Results are compared with the FTIR spectra of the same membrane type in BCA-free HBr/Br_2/H_2O samples at same *SoCs*. Details are explained in the ESI.

2.8. Cycling tests and H_2/Br_2-RFB test cell

Cell tests are performed by galvanostatic cycling with a current density of ±100 mA cm^{-2} in a H_2/Br_2-RFB single cell to evaluate cycling performance of series no. 1 to 4. Only results with electrolytes containing [C6Py]Br are performed. Starting with electrolytes from *SoC* 100 %, the cell test operates in discharge operation followed by a charge process. A Nafion117 membrane with a geometrical active area of 40 cm^2 and a single-sided Pt/C catalyst for the H_2 reactions is used in the cell. The hydrogen half cell is operated in a non-recyclable flow through mode. The feed of dry H_2 has a flow rate of 100 mL min^{-1} during charge and discharge operation with a stoichiometric factor (λ) λ of 3.29. The stoichiometric factor λ defines the ratio of the amount of hydrogen available in the negative half cell and the needed amount of hydrogen

for the discharge reaction. The excess of H_2 and the high loading of the hydrogen electrode with Pt catalyst (3 mg Pt cm^{-2}) prevent limiting processes in the hydrogen half cell and allow a focus on the investigation and monitoring of phenomena of the positive Br_2 half cell. A graphite felt is embedded in a flow frame and is applied as electrode of the positive half cell. The aqueous electrolyte is pumped continuously in flow through mode through the positive half cell felt with a flow rate of 30 mL min^{-1}, while the high density fused salt stays in the tank. Further material and cell information are provided in the ESI. The two phase electrolyte is stored in a sealed glass tank. The cell voltage $E_{Cell\ i\neq0}$ under operation, the redox potential of the electrolyte $\varphi(Br_2/Br^-)_{redox}$ versus the normal hydrogen electrode (NHE), half-cell potentials of the positive bromine half cell $\varphi(Br_2/Br^-)_{i\neq0}$ vs. NHE and the negative hydrogen half-cell potential $\varphi(H^+/H_2)_{i\neq0}$ vs. NHE are determined in parallel during cycling experiments. The setup is shown in the ESI. Between discharge/charge operation during the cycling test the ohmic cell resistances are investigated by means of galvanostatic electrochemical impedance spectroscopy (ESI). From results efficiencies, energy densities and capacities are calculated.

2.9. DFT studies

Density functional theory (DFT) studies are performed to theoretically evaluate the formation of $[BCA]Br_{2n+1}$ ion pairs and to validate measurement results. DFT calculations have been performed using the M062X hybrid functional and 6–311++g** basis set [66], and the D3 correction was used as it is very important to consider the H···Br interactions between Br^- or the polybromides Br^-_{2n+1} and the protons of the two $[BCA]^+$ molecules ($[C2Py]^+$ and $[C6Py]^+$). The solvent effect is considered with the implicit solvent model using the solvent model density (SMD) approach [67] in order to approach experimental reaction conditions in the modelling. All optimized structures are verified to be the minima on the potential energy surface by analyzing the vibrational frequencies. All calculations are performed using the Gaussian16 package [68]. Due to the possibility of various isomers in the formation of the complex, various orientations have been examined.

3. Results and discussion

3.1. Reduction of $[C6Py]^+$ cation concentration in the aqueous solution and compared to $[C2Py]^+$-electrolytes

The aim of this work is to reduce the amount of $[C6Py]^+$ cations in the aqueous solution by transferring those cations completely into the fused salt due to intervening in the solubility equilibrium according to Eq. (1). The concentrations of $[C6Py]^+$(aq) cations as a function of the *SoC* for the excess of Br_2 (+0.00, +0.84, +1.68 and +2.51 M Br_2) are shown in Fig. 2 (points). The results are compared with concentration values of $[C2Py]^+$(aq) cations shown for equivalent electrolyte mixtures (+0.00, +1.68 and +2.51 M Br_2) obtained in a previous work [15] in Fig. 2 (dotted lines).

For the electrolyte without an excess of Br_2 (series no. 1), the concentration of $[C6Py]^+$(aq) decreases strongly and approximately linearly starting from 1.11 M between $0 \leq SoC \leq 40$ %. For $SoC \geq 30$ % in series no. 1, >50 mol% of both $[BCA]^+$ cation types are transferred into the fused salt. Detailed explanation for series no.1 was given in ref. [19].

The excess of Br_2 in the electrolyte (series no. 2 to 4) leads to a further strong decrease of the $[BCA]^+$(aq) cation concentration within the whole *SoC* range, as shown in Fig. 2. $[C6Py]^+$ cations are bound more strongly in the fused salt by lower $[C6Py]^+$ concentrations compared to $[C2Py]^+$ cations for all electrolyte series also for high excess amounts of Br_2. A wider usable BCA-free *SoC* range of the aqueous electrolyte starting from *SoC* 100 % to lower *SoC* values is achieved by using [C6Py]Br compared to [C2Py]Br. BCA-free *SoC* ranges of the aqueous electrolyte are shown in Table 2.

Especially $[C6Py]^+$(aq) cations are only detectable in the aqueous phase within a small *SoC* range. Detection limits of [C6Py]Br and [C2Py]Br are compared in Table 2, as are concentrations of $[C6Py]^+$(aq) and $[C2Py]^+$(aq) at *SoC* 0 %. A bromine excess concentration of +1.68 M Br_2 reduces the maximum $[BCA]^+$(aq) concentration to 32 mM $[C6Py]^+$(aq) compared to a concentration of 225 mM $[C2Py]^+$(aq), leading to a reduction of 97.1 mol% ($[C6Py]^+$) versus 79.5 mol% ($[C2Py]^+$) compared to a total concentration of 1.11 M $[BCA]^+$ in the electrolyte. For an excess of bromine of +2.54 M Br_2, a maximum of 5 mM $[C6Py]^+$(aq) is present (reduction of 99.6 mol%), while for $[C2Py]^+$(aq) a maximum of 67 mM is present within the entire *SoC* range at chemical equilibrium in the electrolyte.

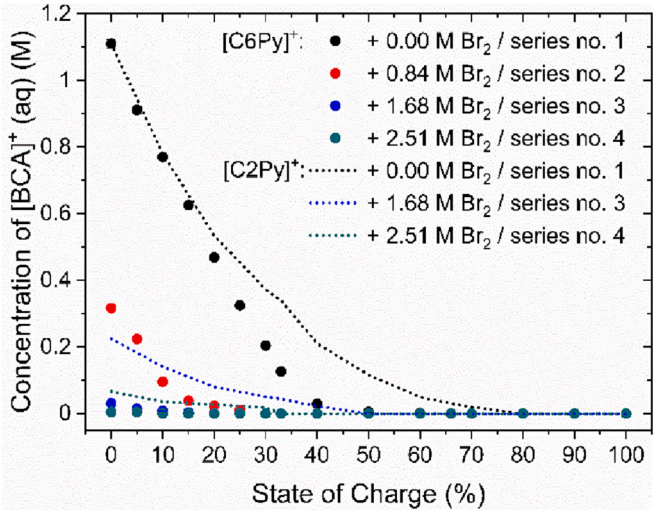

Fig. 2. Concentration of $[C6Py]^+$(aq) cations in aqueous electrolyte phase (dots) depending on the excess bromine concentrations +0.00, +0.84, +1.68 and +2.54 M Br_2 as a function of the *SoC*. For comparison, concentrations of $[C2Py]^+$(aq) cations (dotted lines) under same conditions from [15] are shown for excess Br_2 concentrations of +0.00, +1.68 and +2.54 M Br_2. Values are tabulated in the ESI in Tables S-3 and S-4.

The combination of the strong Br_2-binding BCA [C6Py]Br and in parallel an excess amount of Br_2 leads to a minimum of $[C6Py]^+$(aq) cations in the aqueous phase. In series no. 4 of [C6Py]Br a maximum of only 0.4 mol% of $[C6Py]^+$ vs. 1.11 M $[C6Py]^+$ is present. Negative influences of the $[BCA]^+$ cation on the cell performance shall be reduced and shall allow cycling within the whole theoretical capacity of 179.5 Ah L^{-1} for many cycles compared to [C2Py]Br electrolytes.

3.2. Influence on the Br_2 concentration in the aqueous electrolyte phase

Combining $[C6Py]^+$ cations as a strong Br_2-binding BCA with an excess concentration of Br_2, both are expected to influence the Br_2 concentration in the aqueous electrolyte. To discuss the ability of [C6Py]Br to complex and transfer bromine into the fused salt, the concentrations of Br_2 in the aqueous phase depending on the *SoC* with and without excess amount of bromine are shown in Fig. 3 (dots). For comparison Br_2 concentrations of aqueous electrolytes with [C2Py]Br (dotted lines) from ref. [15] are depicted.

The trend of Br_2 concentrations in [C6Py]Br aqueous electrolytes in Fig. 3 as a function of *SoC* is comparable to the concentration behavior in [C2Py]Br electrolytes from ref. [15] for all series. With increasing *SoC*, the absolute bromine concentration increases (ESI, Table S-2), and Br_2 concentrations in the aqueous phases (Fig. 3) also increase for all electrolyte series up to *SoC* 70/80 % in the aqueous phase (Fig. 3). For higher $SoC > 70/80$ % the concentration of Br_2(aq) decreases. Rising excess amounts of Br_2 in series 1 to 4 lead also to increased concentration of Br_2 in the aqueous phase.

While the objective of lower concentrations of $[C6Py]^+$ cations in the aqueous solution is achieved, the maximum Br_2 concentration at *SoC*

Table 2
Electrolyte properties for bromine electrolytes containing [C6Py]Br as BCA for different electrolyte series with different excess amounts of Br_2 at *SoC* 0 % and comparison with properties for the application of [C2Py]Br from [15] for $[BCA]^+$(aq) concentration at *SoC* 0 %, detection limit of $[BCA]^+$(aq) cations in the form of *SoC* values, Br_2(aq) concentration in aqueous electrolyte solution at *SoC* 20 % and conductivity of the aqueous electrolyte phase at *SoC* 0 %.

Electrolyte series	Concentration of $[BCA]^+$(aq) at *SoC* 0 % (mM)		Detection limit of $[BCA]^+$(aq)/not detectable for *SoC*/%		Concentration of Br_2 (aq) at *SoC* 20 % (mM)		Conductivity of aqueous phase at $\vartheta = 23 \pm 1$ °C and *SoC* 0 %/mS cm^{-1}	
	[C2Py]Br	[C6Py]Br	[C2Py]Br	[C6Py]Br	[C2Py]Br	[C6Py]Br	[C2Py]Br	[C6Py]Br
Series no. 1 (+0.00 M Br_2)	1110	1110	≥80	≥60	116	10	461.1	380.6
Series no. 2 (+0.84 M Br_2)	Not available[a]	317	Not available[a]	≥30	Not available[a]	57	Not available[a]	544.1
Series no. 3 (+1.68 M Br_2)	225	32	≥50	≥20	362	254	681.7	647.3
Series no. 4 (+2.51 M Br_2)	67	5	≥33	≥10	691	612	727.2	716.4

[a] Values concerning electrolyte mixtures containing $[C2Py]^+$-cations used as $[BCA]^+$-cations are adapted from our previous work [15]. In ref. [15] values of concentration of $[C2Py]^+$(aq) at *SoC* 0 %, detection limit of $[C2Py]^+$(aq), concentration of Br_2(aq) at *SoC* 20 % and conductivity of aqueous phase at SoC 0 % with a Br_2 addition of +0.84 M Br_2 have not been investigated and are not available so far for comparison in this work. In this work series no. 2 with an addition of +0.84 M Br_2 is added to investigate the range between a bromine excess of 0 M Br_2 and +1.68 M Br_2.

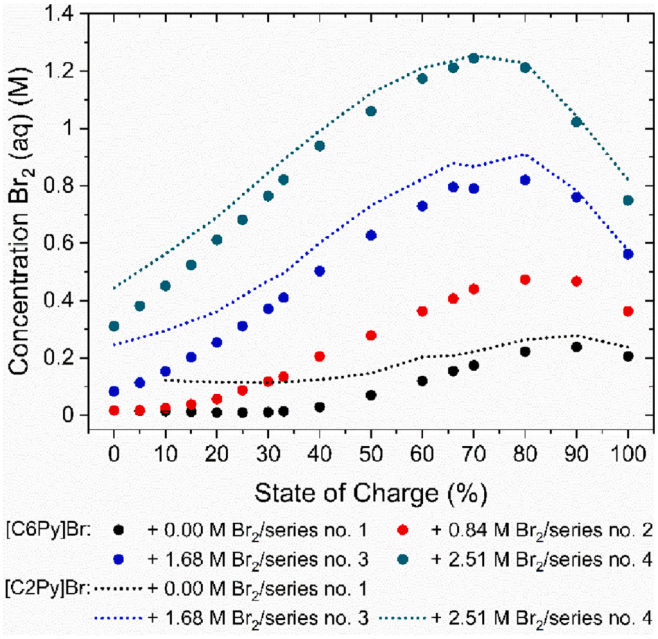

Fig. 3. Concentrations of Br_2 in aqueous electrolyte solution depending on the *SoC* and the excess concentrations of Br_2 (at *SoC* 0 %) for the application of [C6Py]Br (dots) and for comparison of [C2Py]Br (dotted lines). Values for [C2Py]Br are adapted from literature [15]. All concentration values are listed in the ESI in Tables S-5 and S-6.

70/80 % in the aqueous phase of [C6Py]Br electrolytes in the presence of excess amounts of Br_2 is similar to the concentrations of [C2Py]Br electrolytes, even as $[C6Py]^+$ cations with their strong Br_2-binding ability are used. It was expected that $[C6Py]^+$ would lower $c(Br_2(aq))$ also for an excess of Br_2 in the electrolytes much stronger than $[C2Py]^+$ does. For series no. 4, Br_2 concentrations higher than 1 M Br_2 are achieved. However, within the whole *SoC* range [C6Py]Br and [C2Py]Br act as strong Br_2-binding BCAs as only a maximum of 25.6 mol% of Br_2 in series no. 4 (*SoC* 70 %) and only 18.8 mol% of Br_2 in series no. 3 (*SoC* 80 %) are soluble in the aqueous solution compared to absolute Br_2 concentrations at these *SoCs*.

For *SoC* < 70 % the Br_2 concentration in aqueous electrolytes of $[C6Py]^+$ cations are lower compared to the one in electrolytes of $[C2Py]^+$ cations (Fig. 3). The difference in Br_2-concentrations between [C6Py]Br-electrolytes and [C2Py]Br-electrolytes are for each series largest at low *SoC* and become smaller with rising *SoC*. The difference in Br_2-binding strength between [C2Py]Br and [C6Py]Br is evident in this *SoC* range. This is confirmed for concentrations of Br_2(aq) at *SoC* 20 % in Table 2. The concentration difference $\Delta c(Br_2)$ between [C2Py]Br electrolytes and [C6Py]Br electrolytes is highest in series no. 3 at *SoC* 0 % with $\Delta c(Br_2) = 163$ mM. Based on the Br_2 concentrations and concentrations of $[BCA]^+$ cations (Fig. 2) in aqueous solution, the solubility of $[C6Py]Br_{2n+1}$ is lower than for $[C2Py]Br_{2n+1}$ also for bromine excess and strongly depends on *SoC*. For increasing *SoC* ≥ 70 %, the dependence of this property on the chosen BCA decreases and Br_2 concentration only depend on *SoC* and the excess amount of Br_2. The low solubility of Br_2 in the aqueous phase leads to a reduction of the Br_2 concentration [11,15,33]. As a consequence, the Br_2 is transferred and taken up by polybromides in the fused salt phase, which tend to form higher polybromides [15].

Without the application of excess amounts of Br_2, $[C6Py]^+$ cations almost completely remove the Br_2 from the aqueous phase. For *SoC* < 60 % (series no. 1, [C6Py]Br), Br_2 concentrations are below 100 mM. For *SoC* = 20 %, the lowest Br_2 concentration of 10 mM is determined, while for the same electrolyte mixture with [C2Py]Br, there is still 116 mM Br_2 in solution. These low concentrations might lead to mass transport limitation in the cell with rising current densities. Series no. 3 and 4 seem to be of higher interest for using a wide capacity range during performant discharge operation.

In summary, bromine concentrations are decreased for excess amounts of Br_2 with the use of [C6Py]Br only for low *SoC* values, while a limitation of Br_2 concentrations is not achieved for *SoC* > 50 %. Nevertheless, series no. 3 and 4 are of interest for an application in the cell, while in series no. 1 and 2 Br_2 is bound very strong in the fused salt and might lead to a lack of Br_2 in the cell during discharge operation.

3.3. Storage capacity of liquid fused salt

Within the entire *SoC* range Br_2 is primarily stored in the fused salt $[C6Py]Br_{2n+1}$(fs) in high concentrations as shown in Fig. 4 between $4.77 \leq c(Br_2,fs) \leq 11.93$ M due to its polybromides' low solubility in contact with $[C6Py]^+$ cations in aqueous solutions. This corresponds to a capacity of the pure fused salt between 255.7 and 639.2 Ah L^{-1}, by taking into account only the volume of the fused salt. However, the electrolyte is only applicable in the cell when aqueous electrolyte or a combination of both phases is used [23,69]. Concentrations and thus fused salt capacities of the fused salt increase with increasing *SoC* and with rising excess amounts of Br_2 since the absolute amount of Br_2 in the electrolyte increases and Br_2 is mainly transferred into the fused salt. Overall, the concentrations of Br_2 in the $[C6Py]Br_{2n+1}$ fused salt are lower than in $[C2Py]Br_{2n+1}$ fused salt (9.26 to 15.12 M) (Fig. 4). Concentrations of Br_2(fs) in series no. 1 to 4 with $[C6Py]Br_{2n+1}$ are lower compared to the ones in $[C2Py]Br_{2n+1}$ due to a larger radius and volume of the involved $[C6Py]^+$ cations compared to the $[C2Py]^+$ cations. However, as in aqueous electrolytes the Br_2 concentration (Fig. 3) for application of $[C6Py]^+$ compared to $[C2Py]^+$ is lower at low *SoCs* and similar at high *SoCs*, the absolute amount of Br_2 stored in $[C6Py]Br_{2n+1}$(fs) is larger than in $[C2Py]Br_{2n+1}$(fs) also for electrolytes with bromine excess. In conclusion, for applying $[C6Py]^+$ cations there is not less Br_2 transferred into the fused salt, but the concentration is lower in

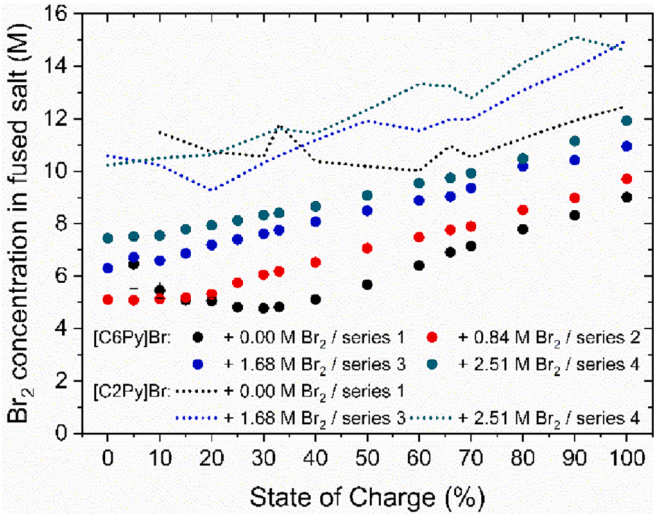

Fig. 4. Concentration of Br_2 in the liquid fused salt $[C6Py]Br_{2n+1}$ (dots) and comparison to the Br_2 concentration in the liquid fused salt of $[C2Py]Br_{2n+1}$ (dotted lines) depending on the *SoC* and the excess of bromine concentration (+0.00, +0.64, +1.68, +2.51 M Br_2) at *SoC* 0 %.

fused salt due to the volumetrically larger organic $[C6Py]^+$ cation compared to $[C2Py]^+$ cations. The fused salt forms the energy reservoir for the positive bromine half cell.

3.4. Interaction of the $[BCA]^+$ cations with Nafion117

In a H_2/Br_2-RFB, cation exchange membranes are employed as protons are carried from the posolyte to the electrode of the hydrogen half cell during the charge process and backwards during the discharge process [70–73]. In this work, Nafion117 membranes are used, which are mechanically stable due to their higher thickness of 175 µm [74,75] and shall reduce crossover towards further electrolyte ingredients. Crossover of $[C6Py]^+$ cations through the membrane is compared to influence on $[C2Py]^+$ cations on these parameters and interaction of $[C6Py]^+$ cations with the membrane is investigated.

3.4.1. Crossover of $[C6Py]^+$ and $[C2Py]^+$ cations

Crossover tests for $[C6Py]^+$ in comparison with $[C2Py]^+$ cations are carried out in a glass diffusion cell on a Nafion117 membrane. Concentrations of $[BCA]^+$ cations in the original BCA-free HBr solution and crossover rates are shown in Fig. 5a.

Both $[C2Py]^+$ and $[C6Py]^+$ cations from the posolyte cross over the membrane, but the concentrations (Fig. 5a – left axis, dots and dotted lines) of $[C2Py]^+$ in the initially BCA-free electrolyte increase more strongly than for the same electrolyte with $[C6Py]^+$ cations. After 48 h, 23.3 mol% of $[C2Py]^+$ (72.3 mM) crossed the membrane, whereas only 10.6 mol% of $[C6Py]^+$ (32.9 mM) crossed during the same time period. From the concentrations, crossover rates of the ions are determined for the investigated time periods (Fig. 5a - right axis and lines). It is remarkable that the transfer rate of $[C2Py]^+$ (approx. 22 to 25 mmol h^{-1} cm^{-2}) is strongly increased within the first 4 h compared to the transfer rate of $[C6Py]^+$ (approx. 3.1 mmol h^{-1} cm^{-2}). With increasing time this difference decreases. Especially the transfer rate of $[C2Py]^+$ decreases and adapts to the transfer rate of $[C6Py]^+$ with approx. 5.6 to 6.2 mmol h^{-1} cm^{-2} in the period between 24 and 48 h. Equal amounts of $[BCA]^+$ cations cross over at 48 h, although the concentration gradients Δc ($[BCA]^+$) across the membrane are different: $\Delta c([C2Py]^+) = 165.4$ mM and $\Delta c([C6Py]^+) = 244.3$ mM. Overall, it appears that $[C6Py]^+$ cations cross over at lower rates due to their size and presumably their lower charge density, even at a larger concentration gradient. $[C2Py]^+$ cations, on the other hand, crosses over in large quantities at the beginning due to smaller size. After 24 h the $[C2Py]^+$ ions bound to the sulphonates in the membrane limit the transport of $[C2Py]^+$.

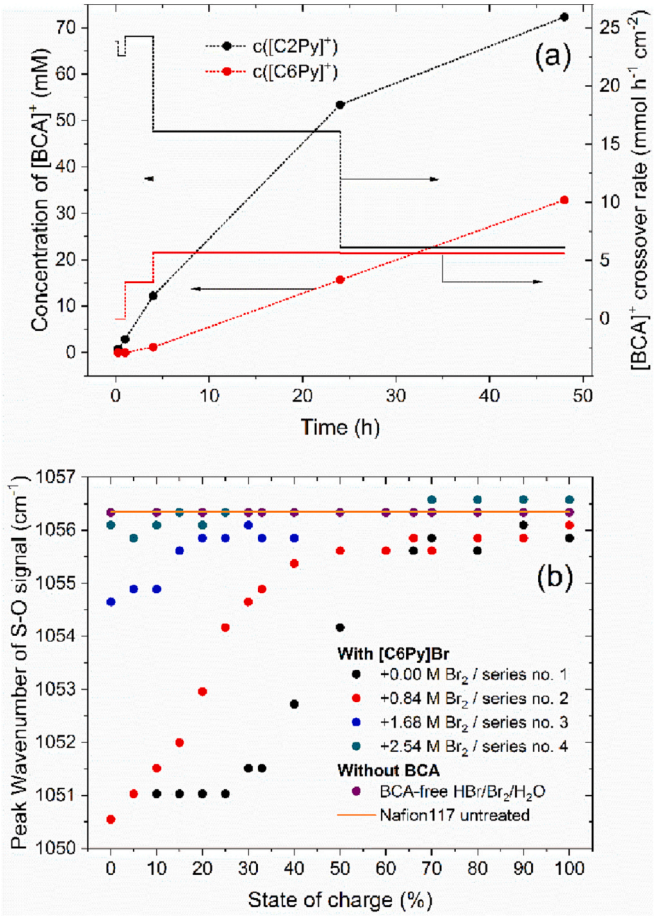

Fig. 5. Effect of $[BCA]^+$ cations in the aqueous electrolytes on the Nafion117 membrane: (a) Crossover of $[C2Py]^+$ and $[C6Py]^+$ cations through the Nafion117 membrane from a 4.5 M HBr/0.31 M $[BCA]^+$ solution into a 4.5 M HBr solution (concentrations left axis) in a glass diffusion cell and crossover rate of the $[BCA]^+$ cations (right axis). (b) Wavenumber of the S—O oscillation peak ($\tilde{\nu}$ = 1056 cm^{-1}) of Nafion117 membrane pieces pretreated in aqueous electrolyte solutions containing [C6Py]Br. (For interpretation of the references to colour in this figure, the reader is referred to the web version of this article.)

3.4.2. Interaction of $[BCA]^+$ cations with sulphonate groups in the membrane

The interaction between the Nafion117 membrane and the $[C6Py]^+$ cations is demonstrated by FTIR measurements on Nafion117 samples placed in aqueous electrolyte solution of all series at various *SoC*. All obtained peaks with corresponding wavenumbers in the FTIR spectra correspond to wavenumbers known in the literature [76–82] for the backbone and side chain of Nafion117 membrane.

The peak with a wavenumber at $\tilde{\nu}$ = 1056 cm^{-1} represents the symmetrical oscillation of the bond between the sulfur atom and the ionized oxygen atom in S—O of the sulphonate group [54,76,77,80,83,84]. The wavenumber position of the peak depends largely on the ions and molecules surrounding the sulphonate group [84,85]. Larger cations with lower charge density forming an addition bond with the sulphonate groups lead to a downshift of the peak wavenumber to lower wavenumbers [84]. The peak position of this peak is shown for all series with [C6Py]Br as a function of *SoC* in Fig. 5b and is compared with Nafion117 membranes that are untreated (Fig. 5b/orange line) or placed in BCA-free $HBr/Br_2/H_2O$ solutions (Fig. 5b/purple dots).

Pretreatment of the Nafion117 membrane with BCA-free HBr/Br_2/H_2O electrolyte results in no change in the peak wavenumber ($\tilde{\nu}$ = 1056.33 cm^{-1}) within the entire *SoC* range compared to the untreated Nafion117 membrane (Fig. 5b). There is no dependence of the wavenumber on the *SoC*. Since all membranes are dried before measurement, there is no difference that can be attributed solely to membranes' different water content.

Membranes pretreated in electrolytes with [C6Py]Br, on the other hand, show a strong downshift in wavenumbers for the oscillation of the S—O group of the membrane (Fig. 5b), which largely depends on the concentration of the $[C6Py]^+$ cation in the aqueous solution. High $[C6Py]^+$ concentrations (Fig. 2) lead to a strong decrease of the peak wavenumber down to $\tilde{\nu}$ = 1050.55 cm^{-1}. For membranes in electrolytes of series no. 1 and 2 at low *SoCs* a strong deviation of the peak wavenumber compared to the peak wavenumber of untreated Nafion117 occurs (Fig. 5b). For series no. 1, a minimum value for the peak wavenumber $\tilde{\nu}$ = 1051.03 cm^{-1} results, which is independent of the concentration of the $[C6Py]^+$ cations in the region $0 \leq SoC$ 25 %. Since the FTIR measurement is performed at the surface of the membrane, a saturation of the sulphonates with organic cations near the surface could occur at this point in the samples with high $[C6Py]^+$ concentrations. As $[C6Py]^+$ cations are large and hydrophobic compared to other quaternary ammonium cations (e.g. $[C2Py]^+$), they might tend to block the channels in the Nafion117 structure, so that there is less transport of molecules, while cations bind more strongly to the sulphonate groups. For series no. 3, however, this influence of $[C6Py]^+$ is much weaker, as the concentrations of $[C6Py]^+$ in the aqueous phase (Fig. 2) are low throughout the *SoC* region. Since series no. 4 is largely free of $[C6Py]^+$ cations, only a deviation smaller than $\Delta\tilde{\nu}$ = 0.5 cm^{-1} from the untreated Nafion117 occurs in the FTIR of Nafion membrane.

It can be seen from the results that $[C6Py]^+$ generally tends to cross over the membrane at a lower rate compared to $[C2Py]^+$, but leads to a strong downshift of the wavenumber of the symmetrical oscillation of the S—O group in the membrane. $[C6Py]^+$ interacts more strongly with the sulphonate group than $[C2Py]^+$ investigated in previous work for with similar concentrations [12], leading to a weaker influence on the peak wavenumber for $[C2Py]^+$. This also confirms that $[C2Py]^+$ cations are transported across the membrane in larger amounts, whereas for $[C6Py]^+$ cations the crossover rates are lower even at larger concentration gradients via the membrane. For the application in the cell, however, it is still essential that the $[C6Py]^+$ concentrations in the aqueous solution are as low as possible, since $[C6Py]^+$ cations, just like $[C2Py]^+$ cations, diffuses into the membrane where they strongly interact with the sulphonates and presumably strongly increases the membrane resistances.

3.5. Conductivities of aqueous electrolytes including [C6Py]Br

The aqueous electrolytes are responsible for charge transport in the electrical field in the bromine half cell. Ionic conductivities of aqueous electrolytes with [C6Py]Br and different excess amounts of Br_2 (series no. 1–4) are shown in Fig. 6 (dots) for $\vartheta = 23 \pm 1$ °C and are compared to (i) reference conductivities of pure HBr/H_2O-electrolytes (orange line) [11,86,87] and (ii) conductivities of the aqueous phases with [C2Py]Br with an excess of bromine (series no. 1, 3 and 4) (dotted lines) from ref. [15]. Conductivities of aqueous electrolytes containing [C6Py]Br reach values between $339.5 \leq \kappa(aq) \leq 778.5$ mS cm^{-1} within the entire *SoC* range (Fig. 6) resulting primarily from the presence of protons from HBr in water during charge transport in the electrolyte by means of the Grotthus hopping mechanism, described in ref. [11, 19, 88].

In the *SoC* range between $0 \leq SoC \leq 60$ % the conductivity of the electrolytes is limited by the presence and rising concentration of the large organic cations of $[C6Py]^+$(aq). The lower the amount of excess Br_2 in solution, the further the conductivity in this range deviates from the BCA-free HBr/H_2O solution (Fig. 6/orange line) by reaching lower values due to rising $[C6Py]^+$ cation concentration. Conductivity values

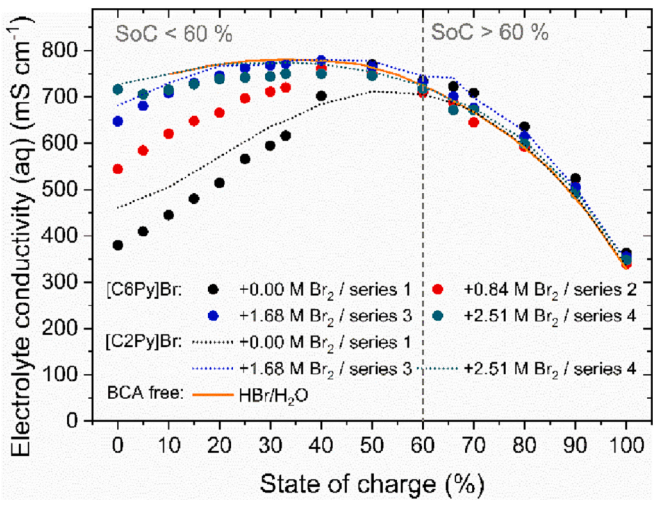

Fig. 6. Conductivity of the aqueous electrolyte phase at $\vartheta = 23 \pm 1$ °C depending on *SoC* and the excess amount of bromine in [C6Py]Br electrolytes (dots), [C2Py]Br electrolytes (dotted lines) from ref. [15] and pure HBr solution (orange line) from ref. [11, 86, 87]. Values are tabulated in the ESI in Tables S-7, S-8 and S-9. (For interpretation of the references to colour in this figure legend, the reader is referred to the web version of this article.)

for *SoC* 0 % are shown in Table 2. The trend is similar with the conductivity behavior of [C2Py]Br electrolytes.

For electrolytes with [C6Py]Br and excess amounts of Br_2 in series no. 3 and 4, conductivities are approximately equal to those of BCA-free HBr/H_2O solutions with high values between $647.3 \leq \kappa(aq) \leq 781.2$ mS cm^{-1} in this *SoC* range. As electrolytes of series no. 3 and 4 are free of $[C6Py]^+$-cations for $SoC > 20$ % and have maximum $[C6Py]^+$ concentrations of 32 mM, the organic cations have limited influence on the aqueous electrolytes' conductivity.

For $60 < SoC \leq 100$ % the conductivity is independent of the $[BCA]^+$ cations and nearly exclusively depends on the HBr concentration, which decreases with increasing *SoC* due to the cell reaction. Detailed explanation is provided in ref. [19].

By applying an excess amount of Br_2, organic $[C6Py]^+$ cations are increasingly transferred into the fused salt and electrolyte conductivity increases as shown earlier for $[C2Py]^+$-cations [15]. As the conductivity of BCA-free HBr/H_2O solutions is reached, a maximum and finite conductivity purely defined by HBr concentration is nearly reached, even when there are low amounts of Br_2 in the aqueous electrolyte. High conductivities in [C6Py]Br electrolytes lead to high performance. Since the electrolyte conductivities are very high, they do not become a limiting factor in cell tests during charge and discharge.

3.6. DFT studies of the interaction between BCA and polybromides

DFT studies are performed to theoretically investigate the interaction between $[C2Py]^+$/$[C6Py]^+$ cations and bromide/polybromides (Br^-_{2n+1}), respectively, and to validate conclusions derived from experimental results. The most stable structures of the bromide and polybromide form in contact with the $[BCA]^+$ cations ($[C2Py]Br_{2n+1}$ and $[C6Py]Br_{2n+1}$ where n = 0–3) are depicted in Fig. 7.

The free energy profiles of the reactions have been calculated using the most likely pathways as [C2Py]Br reacts with Br_2 and forms [C2Py]Br_3 which then further reacts with Br_2 and forms [C2Py]Br_5, [C2Py]Br_7 etc. by calculating the Gibbs free energy change ΔG for the reactions in various intermediate steps. Ion pairing free energies (ΔG) of the respective reaction equilibria of [C2Py]Br, [C2Py]Br_3, [C2Py]Br_5 and [C2Py]Br_7 are shown in Table 3/column 2. In general, similar ΔG values for [C6Py]Br_3, [C6Py]Br_5 and [C6Py]Br_7 in comparison to $[C2Py]^+$ components are obtained (Table 3/column 3).

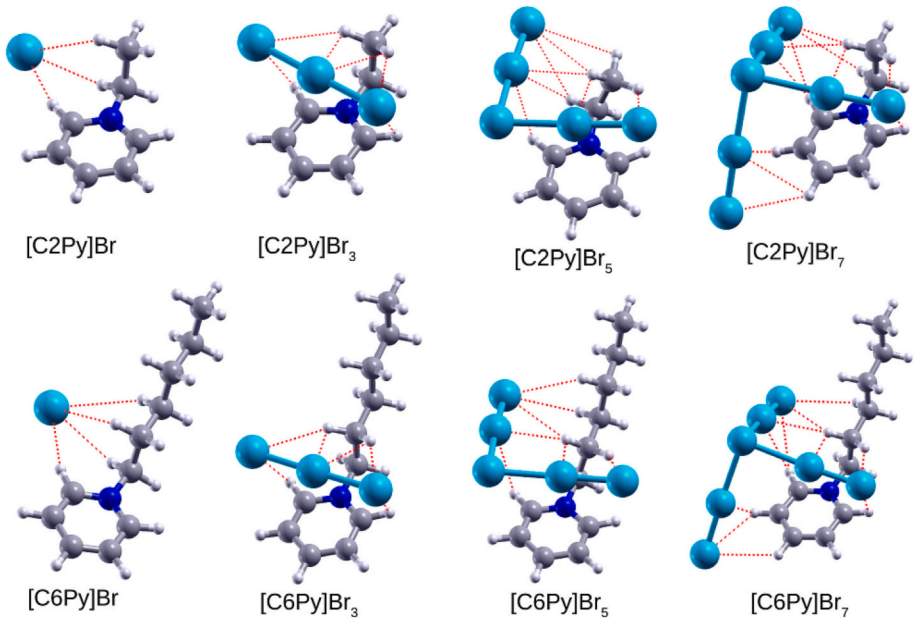

Fig. 7. Minimized structures of the $[C2Py]Br_{2n+1}$ and $[C6Py]Br_{2n+1}$ (where n = 0–3). White, Grey, Blue and Cyan spheres represent H, C, N and Br atoms, respectively. The dotted Red lines represent the Br interactions of the polybromides with the nearest H atoms of the $[BCA]^+$ cations. (For interpretation of the references to colour in this figure legend, the reader is referred to the web version of this article.)

Table 3
Gibbs free energy of ion pairing (ΔG/kJ mol^{-1}) for the ion pairing of $[C2Py]^+$ cations and $[C6Py]^+$ with bromide [BCA]Br (n = 0) and the addition of Br_2 to form tribromides [BCA]Br_3 (n = 1), pentabromides [BCA]Br_5 (n = 2) and heptabromides [BCA]Br_7 (n = 3).

	Ion pairing free energy (ΔG)/kJ mol^{-1}	
	$[C2Py]^+\cdots Br^-_{2n+1}$	$[C6Py]^+\cdots Br^-_{2n+1}$
$[BCA]^+ + Br^- \rightleftarrows [BCA]Br$	3.87	4.72
$[BCA]Br + Br_2 \rightleftarrows [BCA]Br_3$	−34.02	−34.89
$[BCA]Br_3 + Br_2 \rightleftarrows [BCA]Br_5$	5.56	2.15
$[BCA]Br_5 + Br_2 \rightleftarrows [BCA]Br_7$	16.13	13.16

Ionic pairing of $[C2Py]^+$ and $[C6Py]^+$ with bromide to obtain [C2Py]Br and [C6Py]Br, respectively, in aqueous HBr/Br_2/[BCA]Br solution requires energy, as shown by the positive ΔG values (Table 3/column 2 and 3). The bromide form of the salts [C2Py]Br and [C6Py]Br, as is known from previous studies [19], is soluble in aqueous HBr/Br_2 solution at high concentration and prefers to form two solvated ions. In aqueous solutions, solvated ions of [BCA]Br reach the lowest energy values. This is confirmed by the DFT study.

The formation of tribromides [BCA]Br_3 from [BCA]Br is preferred, reaching the lowest free energy values compared to the formation of [BCA]Br, [BCA]Br_5 and [BCA]Br_7 (Table 3). Ion pairing energies ΔG of [BCA]Br_5 compared to [BCA]Br_3 and of [BCA]Br_7 compared to [BCA]Br_5 are more positive compared with [BCA]Br_3 complex formation. In the presence of Br_2 in the electrolyte solution, the [BCA]Br_3 is the most preferred form for ion pairing, followed by [BCA]Br_5 and then [BCA]Br_7. The interaction between the $[BCA]^+$ cations and the polybromides Br^-_{2n+1} which is strongest for tribromides, followed by pentabromides and heptabromides. This behavior appears qualitatively for both molecules and thus is independent of the length of the alkyl side chain. As the absolute Br_2 concentration increases during charging of the battery the majority of Br_2 continues to be stored in the fused salt as the polybromide salt, specifically as Br^-_5 and Br^-_7. However, Br^-_5 and Br^-_7 interact less strongly with the $[BCA]^+$ cations.

The formation of the ion pair of $[C6Py]^+$ and Br^- occurs less preferentially than the formation of [C2Py]Br in aqueous solution, since a higher energy value is determined for [C6Py]Br compared to [C2Py]Br. In all steps, [C6Py]Br reacting with Br_2 is energetically more favourable compared to [C2Py]Br. It is evident from experiments that Br_2 consumption is higher in the presence of $[C6Py]^+$ compared to that in the presence of $[C2Py]^+$, and this is also evident from our computational results. The longer n-hexyl side chain allows a stronger interaction between the negatively charged polybromides Br^-_{2n+1} and the larger number of hydrogen atoms of the n-hexyl side chain compared to the shorter ethyl side chain. Particularly in the presence of Br^-_5 and Br^-_7 in the solution, the $[C6Py]^+$ form of the salt retains the lower energy level compared to the $[C2Py]^+$ cations. As a result, even in the presence of excess bromine, the Br_2, which forms polybromides Br^-_{2n+1} is more firmly attached to the $[C6Py]^+$ compared to $[C2Py]^+$.

3.7. Cycling tests of [C6Py]Br electrolytes

To investigate the cycling ability of electrolytes containing [C6Py]Br in a H_2/Br_2-RFB single cell, galvanostatic cycling tests are performed for all 4 electrolyte series. All electrolytes are discharged starting from a *SoC* of 100 % and then are charged back to *SoC* 100 %. Cycling of electrolytes containing [C2Py]Br have been discussed in ref. [12, 15, 21] and is not shown in this work. Cell voltages as a function of the cycling time (Fig. 8a–d) and ohmic cell resistances as a function of the cycle number before and after discharge operation (Fig. 8f) have been measured for all four electrolytes for up to 12 cycles, respectively. From cell voltages and currents, cycling efficiencies (Fig. 8f) and applicable electrolyte capacities and discharge energy densities as a function of the cycle number (Fig. 8g–h) are calculated to discuss influence of $[C6Py]^+$-electrolytes on the cell performance. Limiting phenomena of the cell are confirmed and discussed based on the half-cell potential of the Br_2/Br^- half cell, the redox potential of the Br_2/Br^-, the overvoltage of the positive Br_2/Br^- half cell, and the residual potential ΔE_{RES}.

3.7.1. Cycling performance results

Although all electrolytes are charged and discharged with the same current density of ±100 mA cm^{-2}, different depths of discharge of the electrolytes starting from *SoC* 100 % are reached, which is visible due to different time scales and cycling times in Fig. 8a–d. A complete cycle with a targeted charge and discharge capacity of 179.6 Ah L^{-1} requires a time period of 8.08 h. However, complete discharge and charge

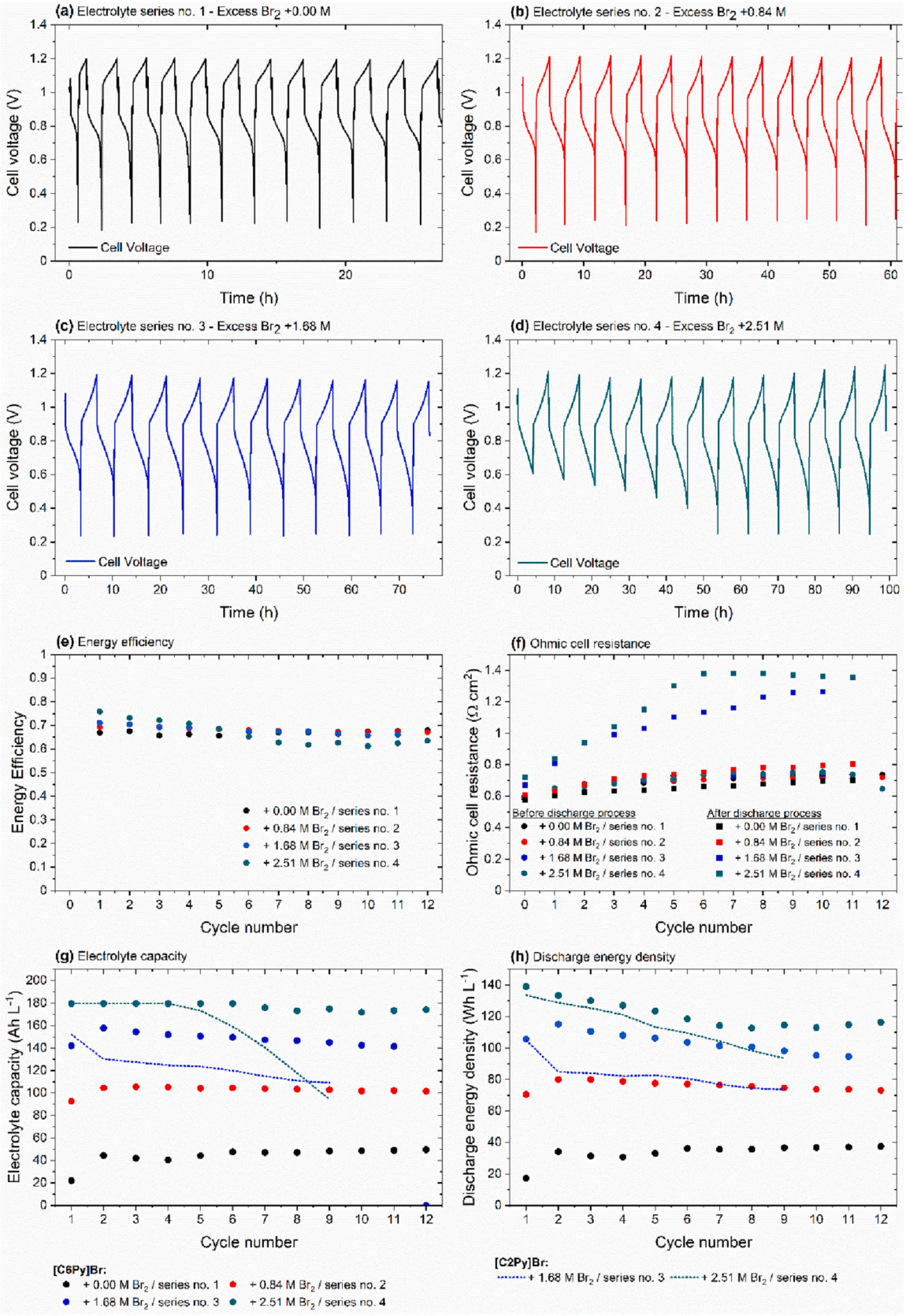

Fig. 8. Galvanostatic cell test at a current density of ±100 mA cm^{-2} for $HBr/Br_2/H_2O$ electrolytes containing [C6Py]Br as BCA with different bromine excess amounts up to 12 cycles: Cell voltage of electrolyte (a) +0.00 M Br_2/series no. 1 (b) +0.84 M Br_2/series no. 2 (c) +1.68 M Br_2/series no. 3 and (d) +2.54 M Br_2/series no. 4 as a function of the time, (e) energy efficiencies as a function of the cycle number, (f) ohmic cell resistance before and after discharge operation as a function of the cycle number and (g) usable charge/discharge electrolyte capacities and (h) discharge energy densities (dots) as a function of the cycle number. For comparison of capacities (g) and energy densities (h) available values for [C2Py]-electrolytes from our own data of ref. [15] are shown (dashed lines).

operation is only achieved for series no. 4 within the first 6 cycles, shown in Fig. 8d, when an excess of bromine of +2.51 M is provided. For electrolyte series no. 1 to 3 (all cycles), as well as for series no. 4 for cycle 7 to 12, the discharge process is terminated in each cycle by a collapse of the cell voltage and reaching the defined lower voltage threshold (0.25 *V*) before reaching the maximum discharge time of 8.08 h, while in series no. 4 (cycle 1 to 6) the discharge process is terminated by reaching the defined maximum discharge capacity.

Due to lower discharge operation times, electrolytes of series no. 1 to 3 offer much lower usable electrolyte capacities as shown in Fig. 8g. Those capacities strongly depend on the excess concentration of bromine in the electrolyte in the different series no. 1 to 4. With decreasing bromine excess from series no. 4 to no. 1, the usable electrolyte capacity decreases significantly (Fig. 8g). However, capacities are approximately independent of the number of cycles for each series. Average values of the usable electrolyte capacities and *SoC* ranges are shown in Table 4. For electrolyte series no. 4 almost the maximum possible usable electrolyte capacity (176.69 Ah L^{-1}) is available throughout the 12 cycles, while for an electrolyte without a bromine access (series no. 1) only 44.20 Ah L^{-1} are usable during operation.

The use of [C6Py]Br as BCA leads to largely steady usable electrolyte capacities. This is not the case for the use of [C2Py]Br electrolytes (Fig. 8g). There, the useful capacity for series no. 3 and 4 decreases more sharply, respectively, as the number of cycles increases. With [C6Py]Br, capacities are achieved which are much more stable and show only low decrease rates. Capacities for $[C2Py]^+$ electrolytes have been extracted from ref. [15].

For all studied electrolytes, the energy efficiency as a function of the cycle number (Fig. 8e) has values between 62.8 and 74.4 % for charge and discharge current densities of ±100 mA cm^{-2}. For the first cycle, the increasing excess of bromine in the electrolyte leads to an increase in energy efficiency between 67.1 and 74.4 %. For electrolytes of series no. 1 to 3, the energy efficiencies are almost constant with average values of $EE = 67.0$ % (series no. 1), $EE = 68.2$ % (series no. 2) and $EE = 68.1$ % (series no. 3). For series no. 4 instead, *EE* decreases slightly between cycle 1 and cycle 8 from 74.4 to 61.7 % and stabilizes around that value for cycle 8 to 12. Besides this trend for series no. 4, the efficiencies are approximately independent of the number of cycles in the investigated range and independent of the excess of bromine in the electrolyte.

While *EE* and usable capacities are approximately steady throughout the number of cycles, variations in ohmic cell resistance occur as a function of the number of cycles and the bromine excess in series no. 1 to 4. Before the first discharge cycle, all cells used for the different electrolyte series have an approximately equal ohmic cell resistance R_{OHMIC} of around 0.60 Ω cm^2. For series no. 1 and 2, the ohmic cell resistance as a function of cycle number slowly increases before and after discharge operation for [C6Py]Br electrolytes, reaching values between $0.70 \leq R_{OHMIC} \leq 0.81$ Ω cm^2 for cycle 12. Instead, for series no. 3 and 4, ohmic resistances of the cell after discharge rise and terminate at much higher values ($1.26 \leq R_{OHMIC} \leq 1.38$ Ω cm^2) compared to their resistances before discharge. Before the discharge process (series no. 3 and 4) the ohmic cell resistance remains low and comparable to resistances of the cell operated with electrolytes of series no. 1 and 2. Since the ionic conductivity of the electrolyte is high (Fig. 6) and electrodes, current collectors and copper plates offer constant ohmic resistances, any change in cell resistance is attributed to changes in the electrolyte composition in the Nafion membrane at the sulphonate groups.

In parallel, the usable discharge energy densities (Fig. 8h) are investigated to combine results of energy efficiency (Fig. 8e), ohmic cell resistance (Fig. 8f) and capacities (Fig. 8g). For series no. 1 and 2, the usable discharge energy densities are largely independent of the number of cycles from the 2nd cycle onward (Fig. 8h), reaching the following average values of 33.49 Wh L^{-1} (series no. 1) and 73.14 Wh L^{-1} (series no. 2). For electrolyte series no. 3, the useable discharge energy density of the electrolyte slowly decreases by about 1.73 Wh L^{-1} $cycle^{-1}$ with increasing cycle number from a maximum value of 115.15 Wh L^{-1}. Electrolytes of series no. 4 reach the full discharge capacity of 179.6 Ah L^{-1} during the first 6 cycles, yet decreasing discharge voltages (Fig. 8d) show that less energy is released. Thus, the usable discharge energy density of the electrolyte decreases continuously from a maximum value of 138.91 Wh L^{-1}, with an energy amount 2.21 Wh L^{-1} $cycle^{-1}$ less available during cycling.

Again, the discharge energy densities for electrolytes with [C2Py]Br of series no. 3 and 4 (Fig. 8h (dashed lines)) decrease stronger than for electrolytes with [C6Py]Br. For electrolyte series no. 3 ([C2Py]Br), the useable discharge energy density of the electrolyte decreases from 104.99 Wh L^{-1} by about 2.87 Wh L^{-1} $cycle^{-1}$. For series no. 4 ([C2Py]Br) the usable discharge energy density of the electrolyte decreases continuously from a maximum value of 133.68 Wh L^{-1}, with an energy amount 5.10 Wh L^{-1} $cycle^{-1}$ less available during cycling.

Taking all these parameters into account, the application of $[C6Py]^+$ cations as BCAs lead to a rather stable performance of the electrolyte in the H_2/Br_2-RFB single cell compared to $[C2Py]^+$-containing electrolytes.

3.7.2. Limitation of the usable capacities in relation to the excess amount of Br_2 during discharge

Series no. 1 to 3 and series no. 4 electrolytes from cycle 7 onwards cannot be completely discharged and charged with capacities of 179.6 Ah L^{-1}. By means of the cell voltages, half cell potentials, redox potential of the electrolyte, the overpotential of the positive Br_2/Br^- half cell and the residual potential ΔE_{RES} shown in Fig. 9 for cycle no. 5 and 6, the origins of this limiting effect are investigated and discussed for each series. For all experiments, the potential of the negative hydrogen half cell remains nearly constant and independent of the charge and discharge process as shown in Fig. 9a–d (blue line), resulting in a cell voltage not limited by the hydrogen half cell performance.

For the application of $[C6Py]^+$ cations as BCA, no formation of low conductivity fused salt in the cell is observed in the experiments. This is evident since no voltage peaks are observed in the first half of charge process in any cell test. For experiments with $[C2Py]^+$ cations in the past charge performance was reduced due to formation of fused salt in the cell [12,15].

For series no. 1 and 2 (Fig. 9a–b), a mass transport limitation is observed during the discharge process caused by a lack of Br_2 in the positive Br_2/Br^- half cell: The discharge process for electrolyte series no. 1 and 3 is terminated by a significant collapse of the cell voltage (black line) and reaching the lower voltage threshold. The collapse of the cell voltage is caused by the sudden and parallel potential drop in the Br_2/Br^- half cell (red line). At the same time, the redox potential (green line)

Table 4
Tabular summary of galvanostatic cell tests for $HBr/Br_2/H_2O$ electrolytes with [C6Py]Br as BCA for various bromine excesses at *SoC* 0 %: Reason for discharge limitation, average applicable *SoC* range, actual usable capacity, average charge and discharge voltages and amount of energy output.

Electrolyte series with [C6Py]Br	Average useable *SoC* range/%	Average useable capacity/ Ah L^{-1}	Average charge cell voltage/ V	Average discharge cell voltage/V	Average change of discharge energy density (Wh L^{-1} $cycle^{-1}$)
Series no. 1 (+0.00 M Br_2)	24.62	44.20	1.118	0.749	1,13
Series no. 2 (+0.84 M Br_2)	57.19	102.66	1.073	0.728	−0.34
Series no. 3 (+1.68 M Br_2)	75.60	135.72	1.018	0.682	−1.73
Series no. 4 (+2.51 M Br_2)	98.43	176.69	1.015	0.640	−2.21

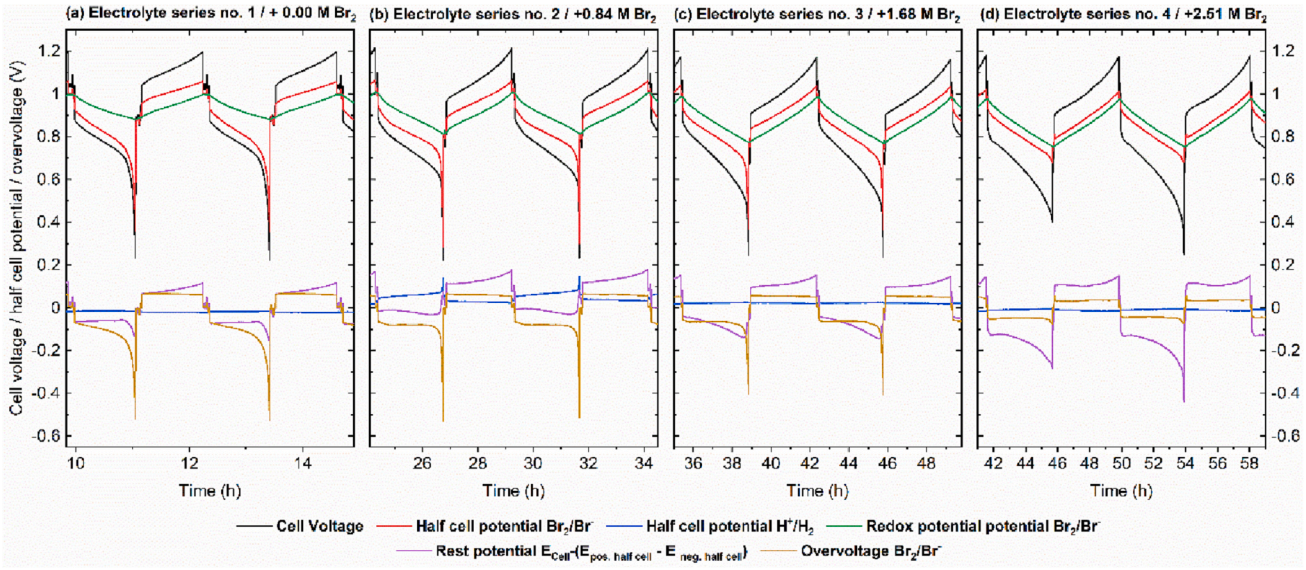

Fig. 9. Results of galvanostatic cycling for cycle no. 5 and 6 for electrolyte series no. 1 to 4 in terms of different voltages and potentials used to study the influences of the bromine/bromide half cell performance and membrane performance on cell performance limitations: cell voltage (black line), positive bromine half cell potential vs. NHE (red line), negative hydrogen half cell potential vs. NHE (blue line), redox potential of aqueous solution Br_2/Br^- electrolyte vs. NHE (green line), positive bromine half cell overvoltage (yellow line) and residual potential ΔE_{RES} (violet line). (For interpretation of the references to colour in this figure legend, the reader is referred to the web version of this article.)

of the electrolyte remains at a higher value. The calculated overvoltage of the positive half cell (yellow line) remains approximately constant throughout the charge and discharge process, except at the moment when the cell voltage collapses. The parallel existence of cell voltage drop, the half cell potential drop of the Br_2/Br^- electrode and the sudden drop of the overvoltage of the Br_2/Br^- half cell (Fig. 9a–b) confirm a mass transport limitation due to a lack of Br_2 as reactant in the positive half cell for series no.1 to 3.

During discharge, Br_2 from the aqueous phase is reduced to form bromide. Due to the strong bromine binding strength of the $[C6Py]^+$ cation, Br_2 is transferred and bound in the fused salt and the Br_2 concentration in the aqueous electrolyte is not sufficient to discharge with a current density of $i = -100$ mA cm^{-2} within the entire capacity range. Those low Br_2 concentrations cause mass transport limitation in the positive half cell resulting in low depths of discharge, low usable capacities and low discharge energy densities of the electrolytes at the given operation conditions (Fig. 8a, b, g, h). However, since this process is completely reversible, the associated parameters show constant values.

Fig. 10b shows the concentrations of Br_2(aq) and $[C6Py]^+$(aq) at equilibrium (both from previous Sections 3.1 and 3.2) and compares them directly to the usable *SoC* ranges and electrolyte capacities in Fig. 10c. Dashed grey lines in Fig. 10b show the *SoCs* in agreement with Fig. 10c, when the lowest possible discharged *SoC* is present after discharge operation from Table 4.

In electrolytes of series no. 1 and 2, $[C6Py]^+$ cations have high concentrations at low *SoCs* (Fig. 10a), but a discharge starting from *SoC* 100 % down to this *SoC* range is not possible under the selected operating conditions (Fig. 10) due to the lack of Br_2 in front of the Br_2 electrode. For equilibrium concentrations $c(Br_2(aq)) \leq 0.21$ M the discharge operation in given cell is not feasible any further (Fig. 10). Thus, the *SoC* range in which cycling is possible involves aqueous electrolytes that are free of $[C6Py]^+$ cations. Due to the BCA-free aqueous electrolyte in the cell the membrane resistance gets only rarely affected by $[C6Py]^+$ cations and stays low (Fig. 8f).

For electrolyte series no. 4 (Fig. 9d), instead limitation of cell performance is caused by interaction of $[C6Py]^+$ cations with the sulphonate groups of the PFSA membrane. The electrolyte is completely discharged from *SoC* 100 % to approx. *SoC* 0 % in the cell and is then charged to reach *SoC* 100 % again. The cell voltage (black line)

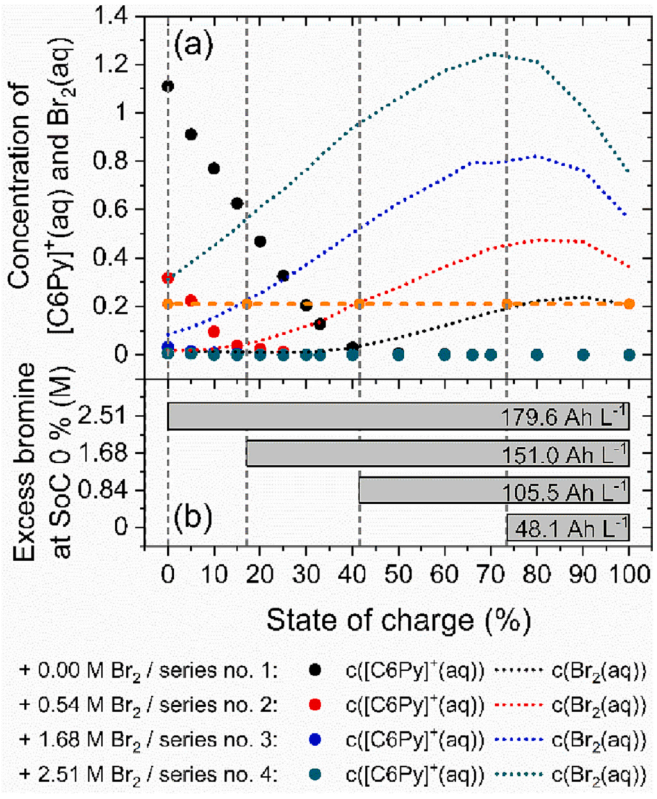

Fig. 10. Summary of results and superposition of individual phenomena affecting cell performance limitation: In (a) concentrations of $[C6Py]^+$ cation and Br_2 in the aqueous solution at equilibrium in comparison with (b) the cyclable *SoC* ranges of the electrolyte including the maximum usable electrolyte capacities for all electrolyte series no. 1 to 4. The orange dashed line and dots show the minimum usable Br_2 equilibrium concentration at 0.21 M Br_2 for all series no. 1 to 4.

decreases during the discharge process, while the half cell potential of the bromine half cell (red line) does not follow the cell voltages' trend. The overvoltage in the positive half cell (yellow line) is approximately constant and no mass transport limitation due to lack of Br_2 is present in this electrolyte. However, the decrease of the residual potential ΔE_{RES} (violet line) is pronounced during the discharge process, indicating a decrease of membrane conductivity. From cycle 7, due to the increasing residual potential ΔE_{RES}, the lower voltage threshold is reached and complete discharge operation is no longer achievable. Ohmic cell resistances after discharge operation increase and terminate at high values throughout the number of cycles (Fig. 8f). Such behavior is indicative of the interaction between $[C6Py]^+$ cations with sulphonate groups of the Nafion117 membrane, drying the membrane due to their hydrophobic cation character (Section 3.4).

While for the application of $[C2Py]^+$ cations in electrolytes it was found that the membrane resistance increases irreversibly with rising cycle numbers [12], the application of the same electrolytes (series no. 3 and 4) with $[C6Py]^+$ as BCA shows that the membrane resistance is decreased during the charge process. The process appears to be reversible when $[C6Py]^+$ is applied for 12 cycles in series no. 3 and 4 (Fig. 8f). We assume that $[C6Py]^+$ is present only in small amounts in the electrolyte during discharge (Fig. 10) and adheres to the sulphonates only at the surface of the membrane. Since crossover of the $[C6Py]^+$ cation across the membrane is much more inhibited than for $[C2Py]^+$ cations (Fig. 5), entry and passage of $[C6Py]^+$ across the membrane is less likely at lower concentrations in the solution. The resistance increases strongly due to the occupancy of the sulphonate with $[C6Py]^+$ cations and their hydrophobic properties in the surface region of the membrane. Although according to Fig. 10a for series no. 4 hardly any $[C6Py]^+$ cations are present, this effect occurs.

In electrolyte series no. 3, both effects of mass transport limitation and rising membrane resistance are superimposed. Indeed, the discharge process of the cell test is primarily terminated by the sudden cell voltage (black line) and potential drop in the bromine electrode (red line) due to a lack of Br_2 (Fig. 9c). However, Fig. 9c shows from the increasing residual potential (yellow line) and the increase in cell resistance in Fig. 8f that there is also a pronounced interaction of $[C6Py]^+$ cations with the Nafion117 membrane, which is reversible and only appears after discharge operation.

For a current density of $i = -100$ mA cm^{-2} at a flow rate of 30 mL min^{-1} it can be seen from Fig. 10b that a minimum Br_2 concentration of 0.21 M is required at equilibrium for all cell tests in aqueous solution. However, by calculation according to Faraday's law, we find that only 1.24 mmol Br_2 min^{-1} is consumed during the reaction, while theoretically 6.30 mmol Br_2 min^{-1} is supplied to the cell at a concentration of 0.21 M Br_2. We assume that the release of Br_2 from the fused salt is severely limited, which means that the necessary amount of Br_2 is not present in the aqueous solution during discharge for low *SoCs*.

4. Conclusions

In this work, for the first time a long side chain quaternary ammonium molecule 1-*n*-hexylpyridin-1-ium bromide [C6Py]Br has been investigated as a bromine complexing additive (BCA) for use in aqueous bromine/hydrobromic acid electrolytes in H_2/Br_2-RFB. Results have been compared with data of 1-ethylpyridin-1-ium bromide [C2Py]Br electrolytes from ref. [12, 15, 19, 23]. To improve electrolyte performance in terms of its capacity and discharge energy density excess amounts of Br_2 have been used in the electrolyte with the aim to store [C6Py]Br completely in the fused salt phase of the electrolyte:

Due to the low solubility of $[C6Py]^+$ cations in contact with polybromides Br^-_{2n+1} in the electrolyte and due to large excess amounts of bromine, $[C6Py]^+$ cations are mainly transferred to the fused salt throughout the whole *SoC* range. Only 0.4 mol% of the $[C6Py]^+$ cations remain in the aqueous electrolyte for solutions including an excess amount of +2.54 M Br_2 (series no. 4). For $[C2Py]^+$ cations in same electrolyte still 6.0 mol% of $[C2Py]^+$ cations remain in the electrolyte. The approximate absence of $[C6Py]^+$ cations in the aqueous electrolyte prevents in cell tests form the disadvantageous formation of fused salt in the cell does not occur and the large increase in membrane resistance. Bromine concentrations in aqueous solution depend on the BCA for $SoC < 50$ % and lead to lower concentrations of Br_2 in $[C6Py]^+$ electrolytes compared to $[C2Py]^+$ electrolytes. However, the excess amount of bromine in the electrolyte dominates the concentration trend. Electrolyte conductivities reach maximum values of pure HBr/H_2O solutions in the presence of excess bromine and do not limit cycling tests.

First time migration of $[C6Py]^+$ cations and $[C2Py]^+$ cations have been investigated and compared in high concentrated HBr electrolyte and both migrate into and even through the Nafion117 membrane utilized, but $[C6Py]^+$ has lower crossover rates compared to $[C2Py]^+$ due to its size and stronger hydrophobic character. Like $[C2Py]^+$ cations, $[C6Py]^+$ cations interact with the sulphonate groups of Nafion117 and lead to decreasing membrane conductivities. However, this increase in resistance is reversible, as the $[C6Py]^+$ cations might only be adsorbed at the membranes' surface within the cycling experiment.

For the first time, the interaction between $[C6Py]^+$ or $[C2Py]^+$ cations and polybromides Br^-_{2n+1} in aqueous HBr/Br_2 electrolytes has been analyzed by means of DFT studies. In this study, the experimental results have been confirmed. Both $[BCA]^+$ cations reach lowest free energy values when interacting with tribromide Br^-_3, which is why $[BCA]Br_3$ formation is the preferred ion pairing. $[C6Py]^+$ interacts more strongly with all polybromides Br^-_{2n+1} and less with bromide Br^- than is the case for $[C2Py]^+$ cations. Due to the intense interaction with polybromides and the lower solubility of $[C6Py]^+$ based salts, $[C6Py]^+$ is preferentially bound in the fused salt phase, leading to an enhanced usability in the electrolytes and the H_2/Br_2-RFB.

In cell tests, it has been shown that the selection of $[C6Py]^+$ cations as BCAs causes significant differences from the application of $[C2Py]^+$ cations: (1) Low amounts of excess Br_2 concentrations of +0 M or + 0.84 M Br_2 (series no. 1 to 2) in the electrolyte lead to limited depths of discharge of the electrolyte due to mass transport limitation of Br_2 in the bromine electrode. The discharge operation is severely limited causing low capacities <120 Ah L^{-1}. (2) The excess of Br_2 of +2.51 M Br_2 (series no. 4) in $[C6Py]^+$ does not lead to a mass transport limitation, which allows a utilization of an average electrolyte capacity of 176.7 Ah L^{-1}. However, even smallest amounts of released $[C6Py]^+$ cations in contact with the membrane lead to a reversible increase of the membrane resistance.

The capacity remains stable over 12 cycles with 176.7 Ah L^{-1} for series no. 4, while for [C2Py]Br electrolytes, there is a significant decrease in capacity of 19.0 % referred to 179.6 Ah L^{-1}. The discharge energy density also decreases more slowly for [C6Py]Br electrolytes from 138.91 Wh L^{-1} by 2.21 Wh L^{-1} cycle^{-1} than for [C2Py]Br electrolytes from 133.68 Wh L^{-1}by 5.10 Wh L^{-1} cycle^{-1}.

Due to the enhanced cycling stability, high and stable electrolyte capacities and discharge energy densities, as well as the reversibility of the increasing membrane resistances, [C6Py]Br is more suitable as a BCA than [C2Py]Br for use in a performant H_2/Br_2 RFB.

CRediT authorship contribution statement

Michael Küttinger: Conceptualization, Methodology, Experimental investigation, Data analysis, Visualization, Writing – Original Draft, Writing – Editing and Review, Supervision of master student, project management. Kobby Saadi: Experimental investigation, Data analysis, Visualization, Writing – Editing and Review. Théo Faverge: Methodology, Experimental investigation, Data analysis Visualization, Writing – Editing and Review. Nagaprasad Reddy Samala: DFT study, Writing – Original Draft. Ilya Grinberg: Writing – Editing and Review, Resources. David Zitoun: Writing – Editing and Review, project management. Peter Fischer: Resources.

Funding

Authors are grateful to the Federal Ministry of Education and Research Germany (BMBF) and the Israel Ministry of Science and Technology (MOST) for financial support of the project through the German-Israeli Battery and Electrochemistry Research Program. We would also like to thank Grenoble-INP/France for a scholarship for the internship period of Théo Faverge.

Declaration of competing interest

The authors declare that they have no known competing financial interests or personal relationships that could have appeared to influence the work reported in this paper.

Data availability

Datasets related to this article can be found in the Electronic Supplementary Information (ESI) of this article.

Appendix A. Supplementary data

Supplementary data to this article can be found online at https://doi.org/10.1016/j.est.2023.107890.

References

[1] K.T. Cho, M.C. Tucker, A.Z. Weber, Energy Technol. 4 (2016) 655–678, https://doi.org/10.1002/ente.201500449.
[2] J. Noack, N. Roznyatovskaya, T. Herr, P. Fischer, Angew. Chem. Int. Ed. 54 (2015) 9776–9809, https://doi.org/10.1002/anie.201410823.
[3] T.V. Nguyen, R.F. Savinell, Electrochem. Soc. Interface (2010) 54–56.
[4] M.L. Perry, A.Z. Weber, J. Electrochem. Soc. A5064–A5067.
[5] Y.V. Tolmachev, Russ. J. Electrochem. 50 (2014) 301–316, https://doi.org/10.1134/S1023193513120069.
[6] K.T. Cho, M.C. Tucker, M. Ding, P. Ridgway, V.S. Battaglia, V. Srinivasan, A. Z. Weber, ChemPlusChem 80 (2015) 402–411, https://doi.org/10.1002/cplu.201402043.
[7] K.T. Cho, P. Albertus, V. Battaglia, A. Kojic, V. Srinivasan, A.Z. Weber, Energy Technol. 1 (2013) 596–608, https://doi.org/10.1002/ente.201300108.
[8] R.S. Baldwin, NASA Technical Memorandum vol. 89862, 1987, pp. 1–26.
[9] R.S. Yeo, D.-T. Chin, J. Electrochem. Soc. 127 (1980) 549–555, https://doi.org/10.1149/1.2129710.
[10] A.Z. Weber, M.M. Mench, J.P. Meyers, P.N. Ross, J.T. Gostick, Q. Liu, J. Appl. Electrochem. 41 (2011) 1137–1164, https://doi.org/10.1007/s10800-011-0348-2.
[11] M. Küttinger, J.K. Wlodarczyk, D. Daubner, P. Fischer, J. Tübke, RSC Adv. 11 (2021) 5218–5229, https://doi.org/10.1039/D0RA10721B.
[12] M. Küttinger, R. Brunetaud, J.K. Włodarczyk, P. Fischer, J. Tübke, J. Power Sources 495 (2021), 229820, https://doi.org/10.1016/j.jpowsour.2021.229820.
[13] G. Lin, P.Y. Chong, V. Yarlagadda, T.V. Nguyen, R.J. Wycisk, P.N. Pintauro, M. Bates, S. Mukerjee, M.C. Tucker, A.Z. Weber, J. Electrochem. Soc. A5049-A5056.
[14] V. Amstutz, K.E. Toghill, C. Comninellis, H.H. Girault, Bulletin Fachzeitschrift und Verbandsinformationen von Electrosuisse und VSE. 10 (2012) 35–40.
[15] M. Küttinger, R. Riasse, J. Wlodarczyk, P. Fischer, J. Tübke, J. Power Sources 520 (2022), 230804, https://doi.org/10.1016/j.jpowsour.2021.230804.
[16] T. Mussini, G. Faita, Encyclopedia of Electrochemistry of the Elements: Bromine, Dekker, New York, 1973.
[17] W. Glass, G.H. Boyle, in: H.R. Linden, G.J. Young (Eds.), Fuel Cell Systems: Symposium Sponsored by the Division of Fuel Chemistry at the 145th and 146th Meetings, American Chemical Society, Washington D. C., 1965, pp. 203–220.
[18] J. Fischer, J. Bingle, J. Am. Chem. Soc. 77 (1955) 6511–6512, https://doi.org/10.1021/ja01629a026.
[19] M. Küttinger, P.A. Loichet Torres, E. Meyer, P. Fischer, J. Tübke, Molecules 26 (2021) 2721, https://doi.org/10.3390/molecules26092721.
[20] S.N. Bajpai, J. Chem. Eng. Data 26 (1981) 2–4, https://doi.org/10.1021/je00023a002.
[21] K. Saadi, M. Kuettinger, P. Fischer, D. Zitoun, Energy Technol. 9 (2021) 2000978, https://doi.org/10.1002/ente.202000978.
[22] M. Kuettinger, M. Cappon, P. Fischer, K. Pinkwart, J. Tuebke, International Flow Battery Forum 2017 - Conference Papers vol. 8, 2017, pp. 106–107.
[23] M. Küttinger, P.A. Loichet Torres, E. Meyer, P. Fischer, Chemistry (Weinheim an der Bergstrasse, Germany) 28 (2022), e202103491, https://doi.org/10.1002/chem.202103491.
[24] W.M. Latimer, Oxidation Potentials, The Oxidation States of the Elements and Their Potentials in Aqueous Solutions, Prentice Hall, New York, 1953.
[25] G. Jones, S. Baeckström, J. Am. Chem. Soc. 56 (1934) 1524–1528, https://doi.org/10.1021/ja01322a022.
[26] D.B. Scaife, H.J.V. Tyrrell, J. Chem. Soc. 0 (1958) 386–392, https://doi.org/10.1039/JR9580000386.
[27] A.J. Bard, R. Parsons, J. Jordan, Standard Potentials in Aqueous Solution: Bromine, CRC Press, New York, 1985.
[28] H.A. Liebhafsky, J. Am. Chem. Soc. 56 (1934) 1500–1505, https://doi.org/10.1021/ja01322a016.
[29] C. Fabjan, G. Hirss, Dechema Monogr. Band 102 (1985) 149–161.
[30] R.O. Griffith, A. McKeown, A.G. Winn, Trans. Faraday Soc. 28 (1932) 101–107, https://doi.org/10.1039/TF9322800101.
[31] W.C. Bray, E.L. Connolly, J. Am. Chem. Soc. 33 (1911) 1485–1487, https://doi.org/10.1021/ja02222a005.
[32] M.S. Sherrill, E.F. Izard, J. Am. Chem. Soc. 50 (1928) 1665–1675, https://doi.org/10.1021/ja01393a021.
[33] J.K. Wlodarczyk, M. Küttinger, A.K. Friedrich, J.O. Schumacher, J. Power Sources (2021), 230202, https://doi.org/10.1016/j.jpowsour.2021.230202.
[34] W. Ramsay, S. Young, J. Chem. Soc. Trans. 49 (1886) 453–462, https://doi.org/10.1039/CT8864900453.
[35] K.J. Vetter, Elektrochemische Kinetik, Springer Berlin Heidelberg, Berlin, Heidelberg, 1961.
[36] D.J. Eustace, J. Electrochem. Soc. 127 (1980) 528–532, https://doi.org/10.1149/1.2129706.
[37] M. Schneider, G.P. Rajarathnam, M.E. Easton, A.F. Masters, T. Maschmeyer, A. M. Vassallo, RSC Adv. 6 (2016) 110548–110556, https://doi.org/10.1039/C6RA23446A.
[38] G.P. Rajarathnam, M.E. Easton, M. Schneider, A.F. Masters, T. Maschmeyer, A. M. Vassallo, RSC Adv. 6 (2016) 27788–27797, https://doi.org/10.1039/C6RA03566C.
[39] D. Bryans, L. Berlouis, M. Spicer, B.G. McMillan, A. Wark, ECS Trans. 77 (2017) 33–36, https://doi.org/10.1149/07701.0033ecst.
[40] D. Bryans, B.G. McMillan, M. Spicer, A. Wark, L. Berlouis, J. Electrochem. Soc. 164 (2017) A3342–A3348, https://doi.org/10.1149/2.1651713jes.
[41] E. Lancry, B.-Z. Magnes, I. Ben-David, M. Freiberg, ECS Trans. 53 (2013) 107–115, https://doi.org/10.1149/05307.0107ecst.
[42] M. Skyllas-Kazacos, G. Kazacos, G. Poon, H. Verseema, Int. J. Energy Res. 34 (2010) 182–189, https://doi.org/10.1002/er.1658.
[43] B.-Z. Magnes, I. Ben David, E. Lancry, M. Bergstein-Freiberg, Additives for Zinc-Bromine Membraneless Flow Cells, Bromine Compounds Ltd., 2013.
[44] K.J. Cathro, K. Cedzynska, D.C. Constable, P.M. Hoobin, J. Power Sources 18 (1986) 349–370, https://doi.org/10.1016/0378-7753(86)80091-X.
[45] W. Kautek, J. Electrochem. Soc. 146 (1999) 3211–3216, https://doi.org/10.1149/1.1392456.
[46] H. Kronberger, C. Fabjan, Monatsh. Chem. 121 (1990) 979–989.
[47] R.A. Putt, M.J. Montgomery, Metal-Halogen Cell Operation With Storage of Halogen Via Organic Complexation External to the Electrochemical Cell, 1977.
[48] A.M. Ajami, F.M. Walsh, D.N. Crouse, Two phase electrolytes used as halogen traps in metal halogen secondary cells and batteries, in: Google Patents, 1976. https://www.google.com.ar/patents/US4065601.
[49] G. Poon, A. Parasuraman, T.M. Lim, M. Skyllas-Kazacos, Electrochim. Acta 107 (2013) 388–396, https://doi.org/10.1016/j.electacta.2013.06.084.
[50] M. Küttinger, J. Noack, R. Elazari, R. Costi, K. Pinkwart, J. Tübke, International flow battery forum, in: Conference Papers, 2017, pp. 46–47.
[51] M.E. Easton, A.J. Ward, B. Chan, L. Radom, A.F. Masters, T. Maschmeyer, Phys. Chem. Chem. Phys. 18 (2016) 7251–7260, https://doi.org/10.1039/c5cp06913k.
[52] T. Schäfer, R.E. Di Paolo, R. Franco, J.G. Crespo, Chem. Commun. (Camb.) (2005) 2594–2596, https://doi.org/10.1039/B501507C.
[53] M.N. Szentirmay, N.E. Prieto, C.R. Martin, J. Phys. Chem. 89 (1985) 3017–3023, https://doi.org/10.1021/j100260a013.
[54] K.M. Cable, K.A. Mauritz, R.B. Moore, J. Polym. Sci. B Polym. Phys. 33 (1995) 1065–1072, https://doi.org/10.1002/polb.1995.090330710.
[55] S.V. Dzyuba, R.A. Bartsch, J. Heterocyclic Chem. 38 (2001) 265–268, https://doi.org/10.1002/jhet.5570380139.
[56] A. Aupoix, B. Pégot, G. Vo-Thanh, Tetrahedron 66 (2010) 1352–1356, https://doi.org/10.1016/j.tet.2009.11.110.
[57] P. Bonhôte, A.-P. Dias, N. Papageorgiou, K. Kalyanasundaram, M. Grätzel, Inorg. Chem. 35 (1996) 1168–1178, https://doi.org/10.1021/ic951325x.
[58] B. Schrader, W. Meier, Raman/IR Atlas Organischer Verbindungen/of Organic Compounds, Verlag Chemie, Weinheim/Bergstr., 1974.
[59] M. Fleischmann, P.J. Hendra, A.J. McQuillan, Chem. Phys. Lett. 26 (1974) 163–166, https://doi.org/10.1016/0009-2614(74)85388-1.
[60] D. Cook, Can. J. Chem. 39 (1961) 2009–2024, https://doi.org/10.1139/v61-271.
[61] W. Vielstich, Z. Anal. Chem. 173 (1960) 84–87, https://doi.org/10.1007/BF00448719.
[62] V.G. 'e. Levich, Physiochemical Hydrodynamics, Prentice-Hall, Englewood Cliffs, N.J., 1962.
[63] F. Opekar, P. Beran, J. Electroanal. Chem. Interfacial Electrochem. 69 (1976) 1–105, https://doi.org/10.1016/S0022-0728(76)80129-5.
[64] S. Treimer, A. Tang, D.C. Johnson, Electroanalysis 14 (2002) 165, https://doi.org/10.1002/1521-4109(200202)14:3<165:AID-ELAN165>3.0.CO;2-6.
[65] A.J. Bard, L.R. Faulkner, Electrochemical Methods: Fundamentals and Applications. Second Edition, 2nd edition, John Wiley & Sons, Inc., United States of America, 2001.
[66] Y. Zhao, D.G. Truhlar, Theor. Chem. Accounts 120 (2008) 215–241, https://doi.org/10.1007/s00214-007-0310-x.
[67] A.V. Marenich, C.J. Cramer, D.G. Truhlar, J. Phys. Chem. B 113 (2009) 6378–6396, https://doi.org/10.1021/jp810292n.

[68] M.J. Frisch, G.W. Trucks, H.B. Schlegel, G.E. Scuseria, M.A. Robb, et al., Gaussian 16, Rev. A.01, Gaussian, Inc., Wallingford, CT, 2016.
[69] L. Amit, D. Naar, R. Gloukhovski, G.J. La O', M.E. Suss, ChemSusChem 14 (2021) 1068–1073, https://doi.org/10.1002/cssc.202002135.
[70] Y.A. Hugo, W. Kout, F. Sikkema, Z. Borneman, K. Nijmeijer, J. Storage Mater. 27 (2020), 101068, https://doi.org/10.1016/j.est.2019.101068.
[71] X. Cheng, Z. Shi, N. Glass, L. Zhang, J. Zhang, D. Song, Z.-S. Liu, H. Wang, J. Shen, J. Power Sources 165 (2007) 739–756, https://doi.org/10.1016/j.jpowsour.2006.12.012.
[72] R.S. Yeo, J. McBreen, G. Kissel, F. Kulesa, S. Srinivasan, J. Appl. Electrochem. 10 (1980) 741–747, https://doi.org/10.1007/BF00611277.
[73] R.S. Yeo, J. McBeen, J. Electrochem. Soc. 126 (1979) 1682, https://doi.org/10.1149/1.2128776.
[74] B. Jiang, L. Wu, L. Yu, X. Qiu, J. Xi, J. Membr. Sci. 510 (2016) 18–26, https://doi.org/10.1016/j.memsci.2016.03.007.
[75] B. Jiang, L. Yu, L. Wu, Mu Di, Le Liu, J. Xi, X. Qiu, ACS Appl. Mater. Interfaces 8 (2016) 12228–12238, https://doi.org/10.1021/acsami.6b03529.
[76] J. Ostrowska, A. Narębska, Colloid Polym. Sci. 262 (1984) 305–310, https://doi.org/10.1007/BF01410469.
[77] J. Ostrowska, A. Narebska, Colloid Polym. Sci. 261 (1983) 93–98, https://doi.org/10.1007/BF01410686.
[78] C. Heitner-Wirguin, Polymer 20 (1979) 371–374, https://doi.org/10.1016/0032-3861(79)90103-4.
[79] H.W. Starkweather, R.C. Ferguson, D.B. Chase, J.M. Minor, Macromolecules 18 (1985) 1684–1686, https://doi.org/10.1021/ma00151a007.
[80] J. Yang, Q. Che, L. Zhou, R. He, R.F. Savinell, Electrochim. Acta 56 (2011) 5940–5946, https://doi.org/10.1016/j.electacta.2011.04.112.
[81] E. Moukheiber, Understanding of the Structure of Perfluorinated Sulfonic Membranes for Fuel Cell, PhD thesis, Grenoble, 2011.
[82] Z. Liang, W. Chen, J. Liu, S. Wang, Z. Zhou, W. Li, G. Sun, Q. Xin, J. Membr. Sci. 233 (2004) 39–44, https://doi.org/10.1016/j.memsci.2003.12.008.
[83] W. Kujawski, Q.T. Nguyen, J. Neel, J. Appl. Polym. Sci. 44 (1992) 951–958, https://doi.org/10.1002/app.1992.070440603.
[84] S.R. Lowry, K.A. Mauritz, J. Am. Chem. Soc. 102 (1980) 4665–4667, https://doi.org/10.1021/ja00534a017.
[85] M. Leuchs, G. Zundel, J. Chem. Soc. Faraday Trans. 2 (74) (1978) 2256, https://doi.org/10.1039/F29787402256.
[86] Petr Vanýsek, in: W.M. Haynes, D.R. Lide (Eds.), CRC Handbook of Chemistry and Physics: A Ready-Reference Book of Chemical and Physical Data. 96. ed., 2015–2016, CRC Press, Boca Raton, Fla., 2015 (5-77–5-79).
[87] W.J. Hamer, H.J. DeWane, Electrolytic Conductance and the Conductances of the Halogen Acids in Water, U. S. Government Printing Office, Washington D. C., 1970.
[88] K.-D. Kreuer, A. Rabenau, W. Weppner, Angew. Chem. 94 (1982) 224–225, https://doi.org/10.1002/ange.19820940335.